

MODELING THE STRUCTURE AND DYNAMICS OF DWARF SPHEROIDAL GALAXIES WITH DARK MATTER AND TIDES

RICARDO R. MUÑOZ¹, STEVEN R. MAJEWSKI¹, KATHRYN V. JOHNSTON^{2,3}

Draft version November 2, 2018

ABSTRACT

Two observed features of dwarf spheroidal (dSph) galaxies — extended light profiles and more or less flat velocity dispersion profiles — have led to competing interpretations over the nature of dSphs: Either the outer characteristics of dSphs are reflecting ongoing tidal disruption, or they are showing the existence of bound stellar “halos” embedded within extended dark matter halos. To accommodate the observed dSph features within the latter interpretation, dSph models now commonly adopt multi-component structures with strongly varying M/L with radius. In contrast, we explore whether the observed features of dSphs can still be accounted for with simpler, mass-follows-light (MFL) models including tidal disruption. As a test case, we focus on modeling the Carina dSph, which resembles other classical dSphs in shape and velocity distribution but presently has the most extensive data at large radius. We find that previous N -body, MFL simulations of (tidally disrupting) dSphs did not sufficiently explore the parameter space of satellite mass, density and orbital shape to find adequate matches to Galactic dSph systems, whereas with a systematic survey of parameter space we are able to find tidally disrupting, MFL satellite models that rather faithfully reproduce Carina’s velocity profile, velocity dispersion profile and projected density distribution over its entire sampled radius. The successful MFL model satellites have very eccentric orbits, currently favored by Cold Dark Matter (CDM) models, and central velocity dispersions that still yield an accurate representation of the bound mass and observed central $M/L \sim 40$ of Carina, despite inflation of the velocity dispersion outside the dSph core by unbound debris. Our survey of parameter space also allows us to address a number of commonly held misperceptions of tidal disruption and its observable effects on dSph structure and dynamics. The simulations suggest that (1) even modest tidal disruption can have a profound effect on the observed dynamics of dSph stars at large radii, and (2) it may be premature to abandon single-component, MFL models, which can successfully reproduce all salient structural and dynamical properties of the Carina (and other) dSph satellites without invoking special timing or viewing perspectives. Satellites that are well-described by tidally disrupting MFL models could still be fully compatible with Λ -CDM if for example they represent a later stage in the evolution of luminous subhalos.

Subject headings: Carina Dwarf – galaxies: stellar content – Local Group – kinematics and dynamics – cosmology : dark matter

1. INTRODUCTION

1.1. *Dark Matter and Tidal Effects in dSphs: Previous Work*

Ever since the work of Hodge and Michie (Hodge 1961a,b, 1962; Hodge & Michie 1969), which suggested that Galactic tides might play an important role in shaping the structure of Galactic dwarf spheroidal galaxies (dSphs), the extent of this tidal influence has been debated. When early precision radial velocity measurements were obtained in the central regions of a number of these dSphs (Aaronson 1983; Mateo et al. 1993; Hargreaves et al. 1994) the relative importance of tidal forces became less clear because the measured high velocity dispersions implied large dark matter contents within dSphs. Using traditional core-fitting methods (e.g., Illingworth 1976; Richstone & Tremaine 1986), central mass-to-light ratio (M/L) values ranging from ~ 5 for Leo I (Mateo et al. 1998; Sohn et al. 2007) to ~ 100 for Draco and Ursa Minor (Armandroff et al. 1995), and even as high as 500 for Ursa Major (Kleyna et al. 2005) and Boötes (Muñoz et al. 2006b; Martin et al. 2007) have been found among Galactic dSph galaxies.

Such large M/L ’s have been difficult to reconcile with the notion that these dwarfs may be tidally truncated (Cuddeford & Miller 1990; Burkert 1997). Moreover, were they to have such high M/L , dSphs would be structurally very different from systems of relatively similar mass and luminosity scale, such as globular clusters and dwarf elliptical galaxies. The notion that dSph velocity dispersions may not directly reflect their mass but may be inflated by various mechanisms has prompted frequent assessment of various alternative dSph structural models — both Newtonian and non-Newtonian (e.g., MOND; Milgrom 1995, Łokas 2001, but see also, e.g., Gerhard & Spergel 1992, Sanchez-Salcedo & Hernandez 2007) — as well as the assumptions built into the core-fitting method for deriving M/L ’s.⁴

For example, among the suggestions within a Newtonian framework, the possible influence of binary stars to inflate velocity dispersions was investigated, but found to be minor (Olszewski et al. 1996; Hargreaves et al. 1996; Kleyna et al. 2002). The influence of velocity jitter in the atmospheres of giant stars is also likely insignificant since such variations rarely exceed $0.5\text{--}1 \text{ km s}^{-1}$ (Bizyaev et al. 2006) or perhaps

¹ Dept. of Astronomy, University of Virginia, Charlottesville, VA 22904-4325 (rrm8f, srm4n@virginia.edu)

² Department of Astronomy, Wesleyan University, Middletown, CT

³ Currently in the Department of Astronomy at Columbia University, New York City, NY (kvj@astro.columbia.edu)

⁴ Core-fitting assumes that these dSphs are in virial equilibrium, their velocity distributions are isotropic, their mass distribution follows that of the light, and their surface brightness, or equivalently, their surface density, are well represented by a King (1962) model.

slightly more (Carney et al. 2003). Other explanations for the seemingly high observed dSph velocity dispersions question the validity of the virial equilibrium assumption, in some cases exploring violations of that equilibrium in the extreme — i.e. proposed models whereby the dSphs are in complete or near complete tidal disruption and their appearance of structural cohesion is an artefact of other dynamical processes that obviate the need for dark matter. Synchronicity between internal stellar and external bulk dSph orbits, for instance, has been proposed as one means to explain the high velocity dispersions and apparent spatial coherence of dSph systems in the resonant orbit coupling models of Kuhn & Miller (1989) and Kuhn (1993). Subsequent work by Pryor (1996) and Sellwood & Pryor (1998) showed that the tidal oscillation mechanism proposed by Kuhn & Miller (1989) is not excited by motion through a realistic, logarithmic Galactic potential, and that the tidally disrupted remnants proposed by Kuhn (1993) would be some ten times larger than the observed dSphs. However, Fleck & Kuhn (2003) have updated the Kuhn & Miller (1989) model and suggest that tidally induced oscillations *can* inflate the velocity dispersion by up to an order of magnitude, although only for a short fraction of a dSph orbital period.

Meanwhile, models of dSphs that are mostly bound but that incorporate the presence of some unbound stars have been partly motivated by the discovery that most of the Galactic dSphs have an extended component beyond their nominal King limiting radius r_{lim} (obtained by fitting a King profile to the inner light distributions; see Appendix A), a feature suggested to be evidence of tidal disruption in these systems (Eskridge 1988a,b; Irwin & Hatzidimitriou 1995; Kuhn, Smith & Hawley 1996; Smith, Kuhn, & Hawley 1997; Majewski et al. 2000). Since these early photometric studies, extended density profile “break” populations⁵ have been found and/or verified in the Ursa Minor (Martínez-Delgado et al. 2001, Palma et al. 2003; Muñoz et al. 2005), Sculptor (Walcher et al. 2003; Westfall et al. 2006), Draco (Wilkinson et al. 2004), Leo I (Sohn et al. 2007) and Carina dSphs (Majewski et al. 2000, 2005; Muñoz et al. 2006a). As has been pointed out in many of these references, the observed “bimodal” dSph structural profiles in these systems look very similar to those produced by N -body simulations of tidally disrupting dwarf galaxies (e.g., Johnston et al. 1999b, Mayer et al. 2002; Choi, Guhathakurta, & Johnston 2002), and in at least one other real dSph case sharing this radial profile shape — the Sagittarius (Sgr) dSph (Majewski et al. 2003) — the secondary, extended population is unquestionably constituted by tidally stripped stars. By analogy it might seem logical to surmise that the other dSph profiles have been shaped by the same disruption processes. However, two frequently cited N -body studies of dSph tidal disruption are typically invoked to argue against this conclusion.

In an attempt to investigate the degree to which Galactic tides can affect the structural and kinematical properties of dSphs — and therefore their inferred M/L — Piatek & Pryor (1995, hereafter PP95) and Oh, Lin, & Aarseth (1995, hereafter OLA95) each carried out numerical simulations of low density satellites containing no dark matter orbiting in a Milky

Way (MW)–like potential. OLA95 modeled low mass satellites ($M_{\text{satellite}} < 2 \times 10^6 M_{\odot}$) orbiting in rather dynamically gentle orbits (eccentricities no greater than 0.5, and perigalactica no closer than 50 kpc) having several perigalacticon passages. OLA95 found that for such systems the satellite density profile becomes flattened in the orbital plane of the galaxy and follows approximately a power-law distribution with long strands of tidally stripped debris formed in some cases. However, OLA95 also found that the velocity dispersion of the unbound, but not yet dispersed, stars was similar to the previous central equilibrium value, implying that the observed high velocity dispersions of dSphs were not being significantly inflated by tidal stripping; OLA95 concluded, therefore, that substantial mass content within the dSphs is unavoidable, even when/if tides are important.

PP95 also studied low mass satellites with masses of $2.7 \times 10^5 M_{\odot}$ and $8.1 \times 10^5 M_{\odot}$ but in rather eccentric orbits (apogalactica of 210 kpc and perigalactica of 30 kpc). Again, rather strongly formed tidal tails were formed in these models, but PP95 found that a significant, artificial (i.e., tidal) increase of the M/L was rarely observed, and, even when found, the phenomenon lasts only briefly (several times 10^8 yr); to invoke this scenario as an explanation for the high observed central velocity dispersion in dSphs would require that we live in a very special time to be observing all dSphs in the same evolutionary phase (near perigalacticon). Thus, PP95 concluded that it is very unlikely that the central regions of dSphs are influenced by tides. They also pointed out that the effects of Galactic tides on dSphs were, for the most part, undetectable, except perhaps for two key features: (1) a velocity gradient (apparent rotation) that should be observed along the major axis of tidally disrupting dwarf galaxies and, (2) a surface brightness distribution that should become more elliptical with radius.

The OLA95 and PP95 studies have been highly influential in reinforcing the notion that tidal disruption is *not* occurring in most dSph systems, since observed dSph galaxies with large central velocity dispersions do not resemble *these particular* models of disrupted systems, which showed tidally induced rotation, distorted morphologies and low central velocity dispersions. Thus has evolved a frequently presented, “bimodal” pair of viewpoints that dSph galaxies *either* have little dark matter and therefore are highly prone to disrupting, *or* that they have high dark matter contents that are incommensurate with tidal stripping⁶ (e.g., Burkert 1997; Kroupa 1997; Gómez-Flechoso et al. 1999; Kleyna et al. 2001; Gómez-Flechoso & Martínez-Delgado 2003; Gilmore et al. 2006; Koch et al. 2007a). However, though not technically flawed, the OLA95 and PP95 studies are highly specialized — the former pertaining specifically to low mass dSphs on rather circular orbits whereas PP95 selected as strawman examples models with M/L so unrealistically low that the satellites do not even survive one perigalacticon passage — so that it is not clear how general are the conclusions of these studies and whether they should continue to be applied to the interpretation of the much better data

⁵ Here, “break” population refers to an empirical description of the density profile where the outer parts of the density distribution seems to “break” to a new, less steep form, departing from a distribution (usually resembling a King profile — see Appendix A) that fits well the inner parts of Galactic dSphs.

⁶ Even when dark matter and tides are included in models, the conclusions lead to a bimodal position. For example, Read et al. (2006b) and Mashchenko et al. (2006) combined tidal interaction with dark matter-dominated, two-component satellite models when studying Galactic dSphs, but concluded that tides are unimportant due to the immense amounts of dark matter in the satellite extended dark matter halos they need to explain the velocity dispersion profiles of dSphs, effectively reinforcing the “bimodal” picture of tides versus dark matter.

we now have on dSph systems. For example, in reality it is likely that dSphs have rather eccentric orbits, as is now known to be the case for at least several of the most recent orbits of the Sgr system (Law et al. 2005), as is expected for the Leo I system (with its enormous radial velocity), as has been measured for several other dSphs (Piatek et al. 2003, 2005, 2006) and as is predicted for cold dark matter (CDM) subhalos (e.g., Ghigna et al. 1998). Moreover, the PP95-adopted $M/L = 1 M_{\odot}/L_{\odot}$ is several times lower than that expected even for an old stellar population with no dark matter, so that the PP95 modeled satellites are much fluffier than would be expected for any dSph system, even ignoring dark matter. While important for demonstrating how dwarf satellites would evolve in specific circumstances, these early models should be used cautiously as guides to understanding real dSph systems on eccentric orbits.

Subsequent to these 1995 studies, Kroupa (1997) and Klessen & Kroupa (1998) were successful in explaining many of the salient features observed in present-day dSphs by modeling them as long-lived, dark matter free, but mostly *unbound* remnant dSph cores of mass only a few percent of the initial satellite mass. In these simulations, the satellites have physical dimensions comparable to Galactic dSphs, they follow the observed linear correlation between surface brightness and total luminosity (Bellazzini et al. 1996), and more importantly, they have inferred (but artificial) M/L as high as 100. However, these models only work if the satellites are in such an eccentric orbit that we see them and their debris more or less projected along the same line of sight. Such alignments are directly testable because the projection of tidal debris is expected to result in a significant spread in color magnitude diagram (CMD) features like the horizontal branch (Klessen & Zhao 2002). This depth effect should be detectable with wide-field photometry, a test carried out by Klessen, Grebel, & Harbeck (2003) with public data from the Sloan Digital Sky Survey (SDSS) in the Draco dSph field. They showed that Draco’s narrow horizontal branch cannot be reproduced by this alignment model and concluded that Draco cannot be the unbound remnant of a disrupted galaxy, and must, therefore, be dark matter dominated. This additional “failure of the tidal model” — though again pertaining to a prediction from a rather highly specialized satellite model — has further promoted a perception that tidal effects are unimportant in dSphs or at least have not affected them significantly (e.g., Kleyna et al. 2001; Walker et al. 2006a; Read et al. 2006b; Gilmore et al. 2006).

More recently, new, large area radial velocity (RV) datasets have become available for the Galactic dSphs and allow for the first time the study of the line of sight velocity dispersion as a function of radius out to (and in some cases well past) r_{lim} . Such extensive velocity data provide new and remarkably consistent constraints on the structure of dSphs. Flat or only slightly rising/declining velocity dispersion profiles have been reported for Sculptor (Tolstoy et al. 2004; Westfall et al. 2006), Draco (Wilkinson et al. 2004; Muñoz et al. 2005), Ursa Minor (Wilkinson et al. 2004; Muñoz et al. 2005), Fornax (Walker et al. 2006a), Sextans (Walker et al. 2006b), Leo I (Sohn et al. 2007; Koch et al. 2007a), Leo II (Koch et al. 2007b, Siegel et al. 2007), Carina (Muñoz et al. 2006a) and Sagittarius (S. R. Majewski et al., in preparation). Previous studies (e.g., Kroupa 1997; Kleyna et al. 1999) have demonstrated that an important difference between a dark matter-dominated, non-disrupting, mass-follows-light (MFL) dSph and a tidally disrupted one is the radial behavior of the veloc-

ity dispersion. The former model would yield a decreasing dispersion with radius, whereas a flat or rising profile is expected for a tidally disrupting dwarf. Thus, tidal disruption provides one explanation for the observed dSph dispersion profiles.

But a third structural possibility, a luminous dSph surrounded by a more extended, mostly dark matter halo is also consistent with the new observations. CDM cosmology-driven models (Stoehr et al. 2002; Hayashi et al. 2003) have shown that the observed dSph velocity dispersion profiles are in good agreement with simulations wherein dSphs inhabit the most massive subhalos ($10^9 - 10^{10} M_{\odot}$) in a Λ -CDM universe, a result that also helps mitigate the so-called missing satellite problem inherent to these cosmologies (Kauffmann et al. 1993; Klypin et al. 1999; Moore et al. 1999). This theoretical result, and the apparent lack of observational evidence supporting tidal stripping as an ongoing process (in the context of the PP95 and OLA95 models), has prompted some more recent studies (e.g., Kleyna et al. 2002; Łokas 2002; Mashchenko et al. 2006; Walker et al. 2006a; Read et al. 2006b) to model the structure of dSphs with two component models (compact stellar and extended dark mass components) to account for the observed dSph velocity dispersion profiles; these two component models use extended DM halos to keep the velocity dispersion profiles flat, and then conveniently create total masses consistent with the enormous total M/L [exceeding 10^3 or $10^4 (M/L)_{\odot}$] required for dSphs to populate the high end of the subhalo mass spectrum in Λ -CDM predictions.⁷ These models explicitly assume that the dwarf satellite is in virial equilibrium throughout its physical extent, and therefore, neglect any tidal influence in the shape of the velocity distribution.

1.2. Goals of this Paper

Against this backdrop of previous work on dSph structure and tidal influences, the present paper has several goals. First, we want to readdress the question to what extent Galactic tides may be affecting dSph galaxies, and, more specifically, reassess the issue of whether other presently observed Galactic dSph satellites may be tidally disrupting along the Sgr paradigm. In some ways our modeling is reminiscent of that by OLA95 and PP95, but we explore a much wider range of satellite orbit, mass and density, and therefore a greater breadth of context to test the character of possible resulting tidal disruption (§2). We return to simpler, more prosaic, one-component, MFL satellite structures because the previous studies have not completely explored the full parameter space possible within this paradigm and therefore (in our opinion) have not definitively ruled out MFL models. It is also possible that MFL dwarfs are a reasonable model for disrupting two-component models, after the outer envelope of extended dark matter has been stripped away (Klimentowski et al. 2007).

But a key difference between our work and the influential OLA95 and PP95 studies is that we explore the case of tidal

⁷ We note that Wilkinson et al. (2004) reported a sudden drop in projected velocity dispersion at about the King limiting radius for the Ursa Minor and Draco dSphs, and Kleyna et al. (2004) reported a similar finding for Sextans. Read et al. (2006b) attempted to model this apparent kinematical feature and concluded that (1) dSph galaxies could have masses as high as $10^{10} M_{\odot}$, and (2) tidal stripping is unimportant interior to ~ 1 kpc, although “tidal shocking” may still be important. However, as has been shown by Łokas, Mamon & Prada (2005) and Muñoz et al. (2005), the reported “cold points” are likely an artifact of binning and of ignoring “velocity distribution outliers”. In one case (Ursa Minor) the result was not confirmed with additional data (Muñoz et al. 2005).

disruption in *dark matter dominated* MFL systems. Also, in contrast to many previous efforts, our models are directly compared to the most constraining, extant data set now available, that for the Carina dSph. While Carina resembles most other dSphs both structurally and dynamically, it offers the advantage that it now has the most extensive spatial and kinematical coverage (Muñoz et al. 2006a) for any dSph outside the Sgr system. We specifically do not address the Sgr dSph because it has already been explored with similar methods and models by Law et al. (2005), and because Sgr has often been argued to be the *exception*, rather than the archetype of Galactic dSphs (e.g., Mateo 1998; Gilmore 2004; Gilmore et al. 2007).

In Muñoz et al. (2006a) we presented empirical findings and arguments that Carina must be forming tidal tails, based on the appearance of the satellite at large radii (e.g., Fig. 1), the implied mass of the system if the outermost Carina stars are bound, and the observed velocity shear along Carina’s major axis (Fig. 2d). The results of our modeling here lend considerable support to the hypothesis that the Carina system is presently tidally disrupting. We show that initially equilibrium, Plummer model satellites on very shocked, radial orbits are transformed into systems with properties remarkably similar to Carina (and other dSph) satellites. In these models, the observed extended populations and the flat dispersion profiles are both a product of tidal debris, despite the presence of dark matter (in an MFL configuration).

While we do not claim to have a *unique* model to describe the nature of the Carina system, our results dispel several common misconceptions about dSph galaxies and tidal disruption often invoked to dismiss the tidal disruption hypothesis: We find that (1) despite the current trend of relying on ever more complex structural models (i.e. more free parameters) to model dSphs, *simple, one-component, tidally disrupting satellite models can adequately reproduce the strong physical constraints provided by existing observations of at least some dSph galaxies.* (2) Our well-fitting tidal disruption model for Carina *even matches the central velocity dispersion and $M/L \sim 40$ of the dSph.* The presence of dark matter and tidal disruption are not mutually incompatible — *MFL, dark matter dominated systems can produce tidal debris streams that are consistent with current observations.* This has already been suggested by our similar modeling of Sgr (Law et al. 2005) and Leo I (Sohn et al. 2007), but now we demonstrate the principle again with a high central M/L dSph system. Thus, attributing ever larger M/L and extended dark matter halos to dSphs to explain their observed outer structure and dynamics may not be necessary. (3) Despite considerable periodic shocking, significant tidal disruption, and the presence of unbound stars near the dSph core, it is found the central velocity dispersion of the satellite still gives a reasonable estimation of its bound mass using the traditional core-fitting methodology. The influence of tides is primarily relegated to the outer parts of the dSph, where the tidal force is strongest (see also Mashchenko et al. 2006). (4) The presence of even a small fraction of unbound stars can influence the observed dynamics of dSphs at large radii. (5) Sgr may not be a unique example of a tidally disrupting dSph among present MW satellites. We conclude by explaining how tidally disrupting systems that are well represented by an MFL paradigm are not necessarily at odds with the current Λ -CDM paradigm.

An ancillary goal of the paper is to demonstrate a methodology to navigate the parameter space of satellite orbit, mass and density to find matches to the observed structure and dy-

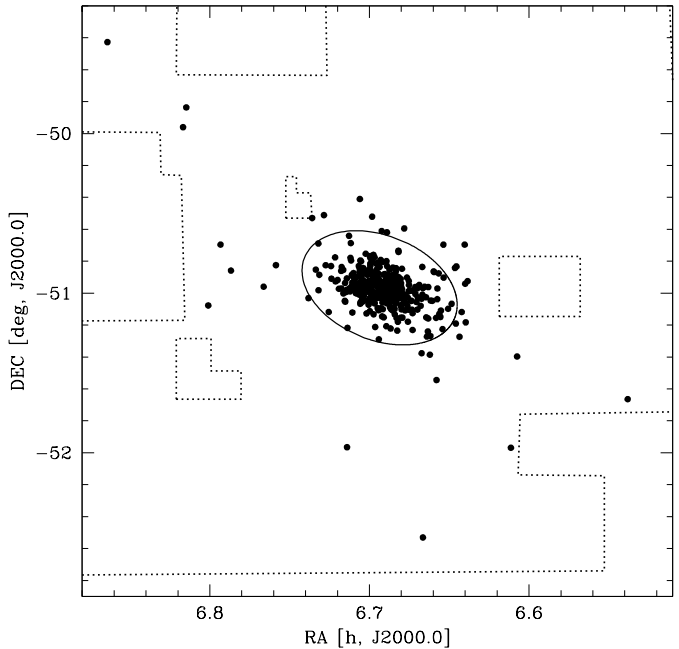


FIG. 1.— Distribution of bona fide Carina RV-members on the sky from Muñoz et al. 2006a.

namics of specific dSph galaxies having dynamical and structural data to large radii using one-component, MFL, N -body simulations. In this case, we apply the methodology to the Carina system, but it is valid for application to any other system with sufficient structural and dynamical data. A second demonstration of the utilization of this methodology has been given in our study of the Leo I system (Sohn et al. 2007).

2. N -BODY SIMULATIONS: MODEL PARAMETERIZATIONS

Several properties of Carina we have observed (Majewski et al. 2000, 2005; Muñoz et al. 2006a) — its substantially extended radial density profile, the highly elongated distribution of RV members, the flat velocity dispersion profile — are consistent with expectations for a satellite galaxy undergoing tidal disruption. But this interpretation is perhaps not readily acceptable or satisfying until a legitimate model or simulation can demonstrate that it is physically possible. Our goal here is to determine under what circumstances (i.e. satellite mass, orbit and density distribution) — if any — the observed Carina velocity and structural characteristics can be imitated by simple, MFL satellites including tidal effects. We have modeled the Carina dwarf with 10^5 particles initially in a Plummer (1911) configuration and with the ensemble orbiting within a static, smooth MW potential. The self-gravitating satellite particles have their mutual interactions calculated using a self-consistent field code (Hernquist & Ostriker 1992). The form of the adopted MW potential, consisting of a Miyamoto & Nagai (1975) disk, Hernquist spheroid and logarithmic halo, as well as the workings of the simulation code is the same as that described in Law et al. (2005). The values for the adopted potential parameters are those used in the Law et al. (2005) simulation of satellite disruption that provided the ‘best fit’ to the spatial and velocity distribution observed for tidal debris associated with the Sagittarius dwarf spheroidal galaxy. In particular, the adopted halo potential is mildly oblate, with minor-to-major

axis ratio of $q = 0.9$.

To navigate the larger parameter space of satellite mass, density and orbit, we first ran a sampling “grid” of satellite parameterizations to zero in on the family of models that best matches the observed Carina properties (§3.1). We then experimented with “fine tuning” models near the “best-matching” part of parameter space in an attempt to improve the match to Carina (§3.2).

The properties of our initial baseline grid of models include the following considerations:

(1) Current satellite position and velocity: The model Carina is placed on orbits that yield a present Galactic location, heliocentric distance R and systemic RV for the satellite similar to that observed for Carina ($l = 262^\circ.1$, $b = -22^\circ.2$, $R = 101$ kpc and $v_{GSR} = 8.0$ km s $^{-1}$).

(2) Satellite mass: In our first tests Carina is represented with initial masses of either 10^6 , 10^7 , or $10^8 M_\odot$.

(3) Orbital plane: Based on previous (e.g., OLA95) and our own preliminary models of Carina-like systems that demonstrate satellite elongation by tides, we set the Carina orbital plane by the position angle of the satellite ($65^\circ \pm 5^\circ$, or roughly $172^\circ \pm 5^\circ$ in Galactic coordinates, from Irwin & Hatzidimitriou 1995). Whether or not this is true, Figure 1 shows that at least empirically the more extended Carina RV members do lie primarily along the central Carina position angle. Preliminary simulations of satellites orbiting with a variety of orbital poles were run, and two (opposite) orbital poles were found to satisfy the generation of debris at the observed PA, namely models with a pole of $(l, b) = (159.3, -12.9)^\circ$ or its antipode at $(339.3, 12.9)^\circ$. Given the symmetry of our model potential and the likelihood that Carina is at its apoGalacticon (see below), we expect similar results with model satellites run on orbits with either of these poles, and elect to run the bulk of our model satellites on orbits with the first pole. Once we find a favored model with this pole, we run a model with the same overall parameters but with the opposite pole (§3.2) to verify the symmetry of solutions. At this point we do not invoke the measured proper motion of Carina by Piatek et al. (2003), since the relative errors in this measurement are large and do not well constrain the direction of motion of Carina (the 95% confidence interval allows a nearly 80° spread in orbital inclination); however we point out some general consistencies of our best fitting model with Piatek et al. results in §3.2.3.

(4) Orbital shape: Because the Carina velocity in the Galactic Standard of Rest convention (v_{GSR}) is nearly zero, Carina must presently be near apogalacticon, near perigalacticon, or be on a nearly circular orbit. Given that the satellite radial velocity must be fixed to that observed, the ellipticity of the model orbits is set by the adopted transverse velocity, v_{trans} for a satellite at the given distance. We have created models characterized by $v_{par} = v_{trans}/v_{circ}$ from 0.3 to 1.0, where v_{circ} is the Galactic circular velocity at the Solar Circle, taken to be 210 km s $^{-1}$ (see Law et al. 2005). The parameter v_{circ} sets the scale of the Galactic mass profile according to the adopted potential. The resulting orbits correspond to (peri/apogalactica) of (15/103) kpc to (85/103) kpc for orbits where Carina is presently at apogalacticon (orbits 1-7 with $v_{par} \leq 0.8$). Orbit 8 with $v_{par} = 0.9$ is relatively circular and orbit 9 with $v_{par} = 1.0$ has Carina near perigalacticon (in an orbit with a 152 kpc apogalacticon). Table 1 summarizes the main properties for these orbits, including peri- (R_{peri}) and apogalacticon (R_{apo}) distance, radial period (T_{rad}), range of peak velocities

observed at perigalacticon (v_{peri}), the timescale of the tidal encounter at perigalacticon ($T_{enc} = R_{peri}/v_{peri}$), the mass of the MW interior to perigalacticon radius (M_{peri}) and the Galactic density (ρ_{peri}) at that radius in our potential. We attempted orbits with v_{par} as low as 0.2 (“orbit 1”), but these have very small perigalactica that cause the orbit to be scattered by the disk potential so that no “typical” orbital properties can be given.

(5) Simulation length and time sampling: For the initial set of models, Carina’s orbit is traced backwards with a single point mass for the lesser of either five radial orbits or 10 Gyr, and then is evolved forward from this point in full N -body mode. We have run most models with 4000 even time steps, but have found that the high perigalacticon velocities for some of the more radial orbits led to conservation of energy problems at perigalacticon, and finer time sampling was implemented as necessary. Energy was conserved at the $\sim 1\%$ level (of the internal satellite energy) when orbit 2 models were run with 64000 time steps, when orbit 3 models were run with 16000 time steps and when all rounder orbits were run with 4000 time steps.

(6) Satellite density: Apart from the mass, we vary the physical scale length, r_0 , of the model satellite distribution, which is initially set to generate a Plummer (1911) model:

$$\Phi = -\frac{GM_{Carina,0}}{\sqrt{r^2 + r_0^2}} \quad (1)$$

The density of the satellite, critical to the degree of robustness of the satellite against Galactic tidal forces and therefore a primary driver in the satellite disruption rate, is set by the initial mass, $M_{Carina,0}$, and scale, r_0 of the satellite. To maintain a constant mass density, the physical scale is sized nominally as

$$r_0 = 0.9(M_{Carina,0}/10^9 M_\odot)^{1/3}. \quad (2)$$

However, to vary the disruption rate, we adjust the scale by up to a factor of five (i.e., density varied by more than a factor of 100) at each adopted satellite mass. In all cases, the initial Plummer-configured satellite is allowed to equilibrate outside the MW potential before being introduced to the potential at the apogalacticon of the orbit.

In summary, our initial grid of 80 models has been constructed with three different satellite masses, with three or four different scale lengths per mass, and with eight different orbital shapes (orbits 2-9). Further explorations of satellite parameter space (§3.2) include additional combinations of mass, scale, number of radial periods run in the potential, and number of time steps in the integration. These extra models pertain primarily to orbit 2 and 3 models (which are found to give the best matches to the data, as shown below). In the end, nearly 200 different N -body simulations to model the Carina dwarf galaxy were run on a nearly devoted Sun Blade 1500 workstation, requiring approximately 6, 24, or 96 hours to run simulations having 4000, 16000 and 64000 time steps, respectively. Table 2 summarizes most of the combinations we have run by scale and mass, with each table entry indicating which orbit shapes were run for a particular mass and scale (and with the bold-faced entries representing the initial parametrization grid of 80 models). Asterisks indicate when a combination of mass, scale and orbit were run for different numbers (e.g., 1, 2, 3, 4, 5) of total radial orbits.

3. RESULTS

TABLE 1
PROPERTIES OF MODEL ORBITS

orbit	v_{par}	R_{peri} (kpc)	R_{apo} (kpc)	T_{rad} (Gyr)	v_{peri} (km s ⁻¹)	T_{enc} (Myr)	M_{peri} (M _⊙)	ρ_{peri} (M _⊙ kpc ³)
1	0.2	< 10	> 145	(not stable)				
2	0.3	15	103	1.46	360-440	32.6	1.90×10^{11}	2.47×10^6
3	0.4	22	103	1.56	310-380	55.3	2.41×10^{11}	1.22×10^6
4	0.5	34	103	1.67	250-350	92.8	3.29×10^{11}	4.96×10^5
5	0.6	48	103	1.85	245-285	160.9	4.50×10^{11}	2.41×10^5
6	0.7	64	103	2.05	222-250	244.6	5.39×10^{11}	1.32×10^5
7	0.8	85	103	2.28	210-227	357.8	6.81×10^{11}	7.41×10^4
8	0.9	95	124	2.71	198-222	408.9	7.48×10^{11}	5.91×10^4
9	1.0	103	152	3.06	218-236	417.0	8.02×10^{11}	5.01×10^4

3.1. Results from the Initial Grid of Satellite Parameterizations

For analysis of our initial grid of simulation parameterizations we adopt as primary discriminants for the “success” of a model its ability to match simultaneously (1) the observed velocity dispersion trend as a function of major axis and radial distance from satellite center, (2) the general shape and size of the Carina radial density profile, and (3) the mean projected velocity along the major axis of Carina. Figure 2 shows these observed constraints, with data taken from Muñoz et al. (2006a).

However, before moving directly to the best fitting models for Carina (see §3.1.4), we take advantage of the fact that our systematic exploration of satellite parameter space leads to results that are useful in a more general context, revealing trends in the nature of satellite tidal disruption that are helpful for understanding the observational properties of tidal debris and disrupting satellites. To keep the scope of this more general discussion to a manageable level, we limit our discussion primarily to the nature of the models as they appear at the distance of Carina, which is at apogalacticon for orbits 1-8 and at perigalacticon for orbit 9. We make this simplification because Carina’s distance is more or less typical for the classical Galactic dSphs, and satellites on elliptical orbits spend more time near apogalacticon than in any other orbital phase.

3.1.1. General trends

To illustrate the general properties of the model satellites in our initial grid we have elected to show, first, the salient features of three satellites of the same mass, $1 \times 10^6 M_{\odot}$, but of different scale lengths (or, equivalently, densities) evolved in our Galactic potential. As we have done for the real Carina data in Figure 2, we show in Figure 3 for the models with two different densities (a) the projected number density profile, the velocity dispersion profiles as a function of both (b) radial distance from the center of the satellite and (c) position along the major axis (normalized to r_{lim}), which we characterize as a function of Galactic latitude, b (since this is a good approximation to the major axis for Carina’s position angle), and (d) the mean projected velocity along the major axis. These properties are shown for four different orbital shapes, from very eccentric ($v_{par} = 0.3$) to rather circular ($v_{par} = 1.0$). In all models at least some degree of tidal disruption occurs and tidal debris dominates the structure and dynamics at large radii.

Some primary sweeping trends are demonstrated in Figure 3. For example, the central velocity dispersion remains almost unaltered by tides (in the sense that its value does not inflate) until the satellite is near complete destruction whereas, at large radii, the velocity dispersion highly correlates to the

degree of tidal stripping (see also Fig. 6). In fact, as found by OLA95, as long as the satellite retains a predominantly bound core, the value of the central velocity dispersion correlates with the instantaneous bound mass of the satellites. In the cases where the system is completely disrupted (i.e., indicated in the figure by having 0% bound mass today), a totally flat velocity dispersion profile is observed, and the magnitude of the dispersion is no longer correlated to the starting mass, but is also influenced by the initial satellite density and orbital shape. Density distributions, on the other hand, seem to be, for the most part, only mildly affected by the degree of tidal disruption when compared to the velocity dispersion profiles for a given mass/density/orbit combination. The main effect of tidal disruption on the density profiles is for the dSphs to develop an extended component that “breaks” from the initial Plummer configuration, as has already been found in previous studies (e.g., Johnston et al. 1999b; Read et al. 2006b; Klimentowski et al. 2007). An overall enlargement of the satellites occurs only when the systems are near destruction, after which they lack a core in the density profile and present a rather flat spatial distribution.

The general appearance of the debris for low eccentricity orbits is illustrated in Figure 4, where we show the $X_{GC} - Y_{GC}$ and $Z_{GC} - Y_{GC}$ Cartesian projections (centered on the Galactic center) for a model with an initial mass of $1 \times 10^7 M_{\odot}$ in two different, rather benign orbits. Tidal debris released at different times is represented by different colors, with the yellow particles marking the presently bound population. The upper and lower panels show the model in a $v_{par} = 0.8$ (nearly circular) and $v_{par} = 0.5$ (3:1) orbit respectively. In both cases, rather narrow, coherent debris streams are formed.

In contrast, Figure 5 shows the $X_{GC} - Y_{GC}$ and $Y_{GC} - Z_{GC}$ Cartesian projection of two $1.0 \times 10^7 M_{\odot}$ satellites of different densities in a very radial orbit ($v_{par} = 0.3$ and $R_{peri} = 15$ kpc) after five perigalacticon passages. The upper panels show a model with a scale of $r_0 = 0.280$ kpc (model 142) and the lower ones a model with $r_0 = 0.194$ kpc (model 102) — i.e. lower and higher density respectively. In both cases the debris is more broadly dispersed, but while model 102 retains a predominantly bound core after five orbits, model 142 has been completely disrupted and lacks a core in the density profile (a property observed in all of our model satellites that have been completely destroyed). As Figures 4 and 5 demonstrate, for a given orbit and mass, the mass-loss-rate is driven by the density of the satellite (Johnston, Hernquist, & Bolte 1996; see also Figure 6, where the density is kept constant and the mass-loss-rate stays the same for a given orbit, even as mass is varied).

Other basic trends depend heavily on the orbit shape, e.g., more circular, rather gentle orbits (apo/perigalacticon ratio no

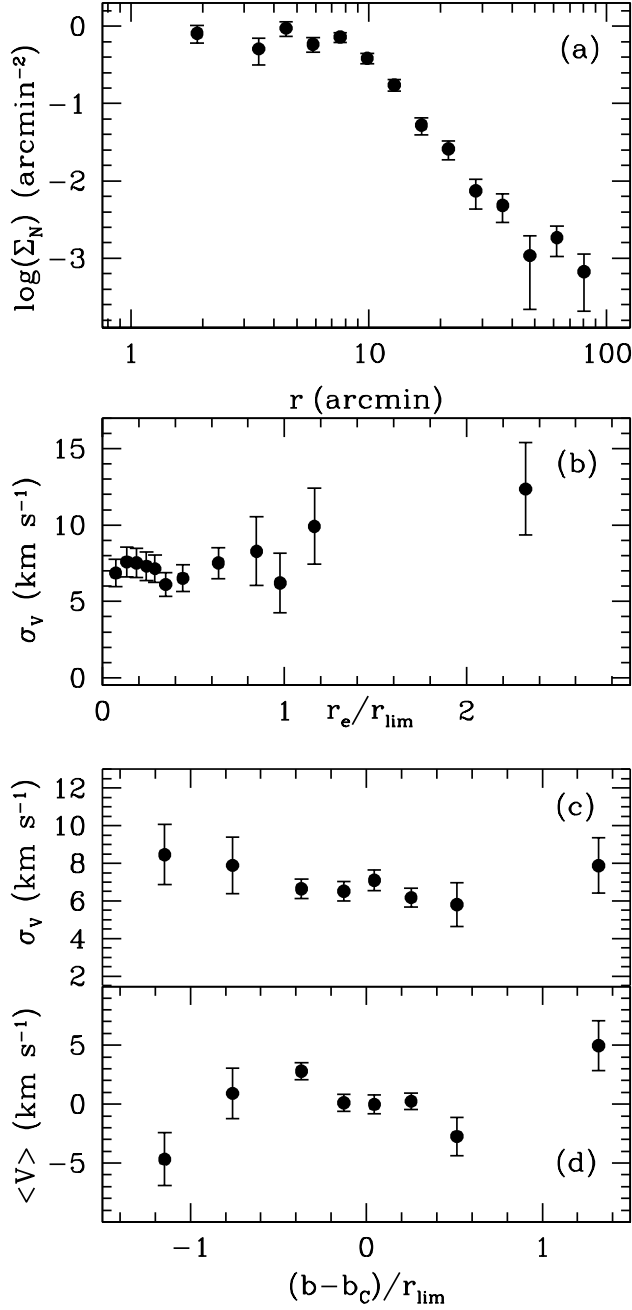


FIG. 2.— (a) Number density profile for the Carina dSph. (b) Observed velocity dispersion as a function of radial distance from the Carina’s center, normalized to r_{lim} . (c) Observed velocity dispersion as a function of Galactic latitude, b , which is a good proxy for the major axis of Carina. We shift the abscissa to be centered on the Galactic latitude of the center of Carina, b_c . (d) Observed mean projected velocity as a function of major axis distance. All data from Muñoz et al. (2006a).

greater than 3:1) versus more energetic, rather eccentric orbits. These results are summarized in Figure 6, which shows the density, mean velocity and velocity dispersion trends for three disrupting satellites of different masses (1×10^6 , 1×10^7 and $1 \times 10^8 M_\odot$) in two different orbits ($v_{par} = 0.8$, left panels; $v_{par} = 0.3$, right panels), this time with central density kept constant (by adjusting the satellite scale to track the cube root of the mass according to Eq. 2) in order to explore the trends

with mass.

After five orbits (or, alternatively, 10 Gyrs, see §2.1), most of the initial mass still remains bound for model satellites in gentle orbits (left panels of Figure 6), regardless of their initial masses. At the same time, all of the simulated satellites in these orbits experienced some degree of tidal stripping that leads to extended spatial components populated by tidal debris. The left panels in Figure 6 show that model satellites with large perigalacticon distances and almost circular orbits ($R_{peri} = 85$ kpc and $v_{par} = 0.8$) undergo relatively modest tidal stripping and their velocity dispersion trends are found to *decline* over degree (kpc) scales, as expected for mostly bound systems (containing particles on predominantly non-circular internal orbits) where the velocity dispersion is the highest at the center and then decreases at large projected radii. However, the velocity dispersion at large radii still departs from the initial, unperturbed value, indicating some tidal heating of the bound population at large radii.

As the orbits become less circular (and the perigalactica smaller), tidal stripping becomes more vigorous and more unbound particles are produced. The right panels in Figure 6 show how tidal debris (unbound particles) generally produce flat or rising dispersion profiles at large radii from the dSph center. In fact, the size of the RV dispersion in the tails correlates with both the mass of the satellite and the orbital shape as long as the satellite retains a predominantly bound core; this is as was found in the modeling of the Sgr system (Law et al. 2005), and was, in fact, one way that was used to constrain the mass of the Sgr system in that study.

A key feature demonstrated by these radial orbit models — indeed by all models retaining bound cores (e.g., in Figures 3 and 6) — is that the central velocity dispersion is still dominated by the bound population even when the outer parts have greatly inflated velocity dispersions. Thus Galactic tides have little effect on the inferred central M/L , even in systems with high disruption rates. However, a radial rise to a *higher* velocity dispersion is also a characteristic product of the unbound component in these radial orbit models. This rise in velocity dispersion can happen well within the limiting radius of the bound system, reflecting the presence of unbound particles quite near the center of the satellite. To illustrate this, in the left panels of Figure 7 we show the spatial distribution (in Galactic coordinates) of particles near the limiting radius for a model in an eccentric orbit ($1 \times 10^7 M_\odot$, $r_0 = 0.194$ kpc, $v_{par} = 0.3$). Panels from top to bottom show particles that have become unbound in successive orbits, with the top panel showing the presently bound population. This figure demonstrates that, in general, the centralized tidal debris responsible for inflating the velocity dispersion radially, is dominated by the “puff” of debris released on the last perigalactic impulse, although particles unbound from prior perigalactica can linger near the dSph center for many orbits. For comparison, the right panels of Figure 7 show the same feature but for the model satellite in a more benign orbit ($v_{par} = 0.8$) where the tidal debris dissipates much more quickly.

3.1.2. Tidally Induced Rotation?

PP95 pointed out that the most unique and readily observable consequence of tidal disruption is tidal shear that resembles solid-body rotation along the major axis of the dSph. To compare our results to these expectations, the lower panels of Figures 3 and 6 show the mean projected velocity along the major axis distance for the same models shown in the upper panels. Satellites in nearly circular orbits show, in general,

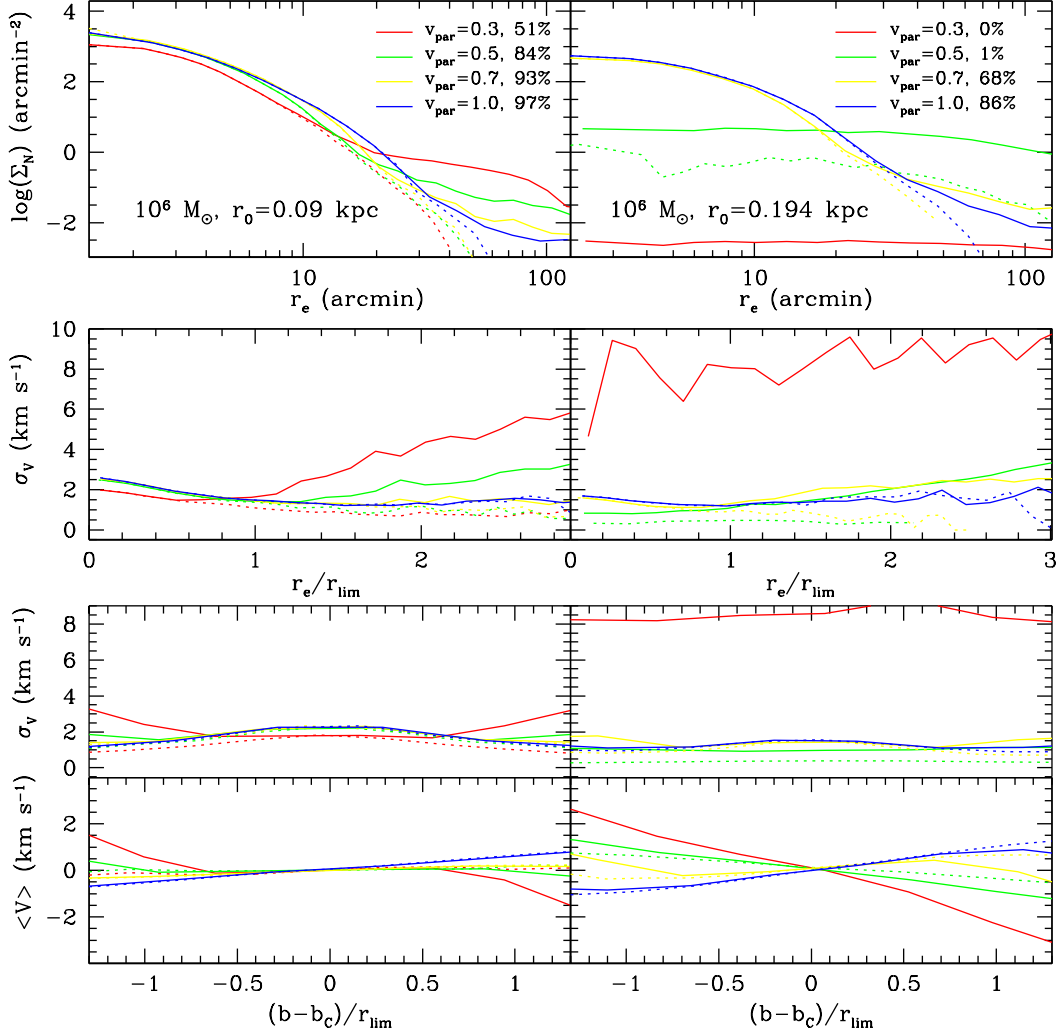


FIG. 3.— From top to bottom: Projected number density profiles, velocity dispersion profiles as a function of radial distance and distance along the major axis (characterized as a function of Galactic latitude and normalized to the respective r_{lim}) and mean projected velocity along the major axis for (*left panels*) model satellite of mass $1 \times 10^6 M_{\odot}$ and scale length of $r_0=0.090$ kpc, in different orbits ($v_{par} = v_{trans}/v_{circ}=0.3$, red lines; 0.5, green lines; 0.7, yellow lines and 1.0, blue lines), and (*right panels*) model satellite of mass $1 \times 10^6 M_{\odot}$ in the same orbits as the left panels, but this time with scale length of $r_0=0.194$ kpc. The percentage numbers represent the fraction of bound mass remaining at the end of the simulation. Solid lines represent all particles while dotted lines show the behavior of the bound particles only.

a smooth velocity gradient within their r_{lim} (e.g., Fig. 6, left panels). However, this small velocity gradient is not a result of Galactic tides (there is only a small degree of tidal disruption suffered by satellites in these orbits) but is predominantly a result of the line-of-sight projection of the satellite mean velocity along the orbital path. On the other hand, satellites in more radial orbits do more strongly show the effect described by PP95 (e.g., Fig. 6, right panels). While satellites that have been completely destroyed show, for the most part, a smooth gradient along the major axis, satellites on more radial orbits that retain at least some bound core show a “rotation” (*S*-shape) signature like that described by PP95. However, it is important to note that this signature is observable mostly outside the r_{lim} of the satellite core, whereas within r_{lim} the magnitude of the signal is typically relatively modest — e.g., small compared to the central velocity dispersion. In these cases of satellites with bound cores, the bound component shows almost no signature of tidal shear and the “rotation” is reflected only in the unbound particles (thus, this “shearing” or “rota-

tion” is really just a reflection of how the tidal debris with its net angular momentum and energy is organizing in response to the MW potential). These results suggest that, while apparent rotation can be a consequence of tidal stripping, as suggested by PP95, for satellites that are not completely destroyed this effect can occur well outside the typical radii to which most current RV surveys of dSphs have been limited. Thus, in most cases the PP95 signal cannot be counted on as evidence for lack of tidal effects since *the rotation would generally not be expected to be seen*, or, if detected, it would likely be deemed as “statistically insignificant” in most studies. We return to this point in §4.1.

3.1.3. Time Dependence of the Satellite Properties

As mentioned in §1.1, a primary problem with previous modeling of tidally disrupting, low M/L satellites is that any successful matches to observed dSph satellites depends on catching these systems in one particular phase of evolution. However, in all cases we have explored, save those where the

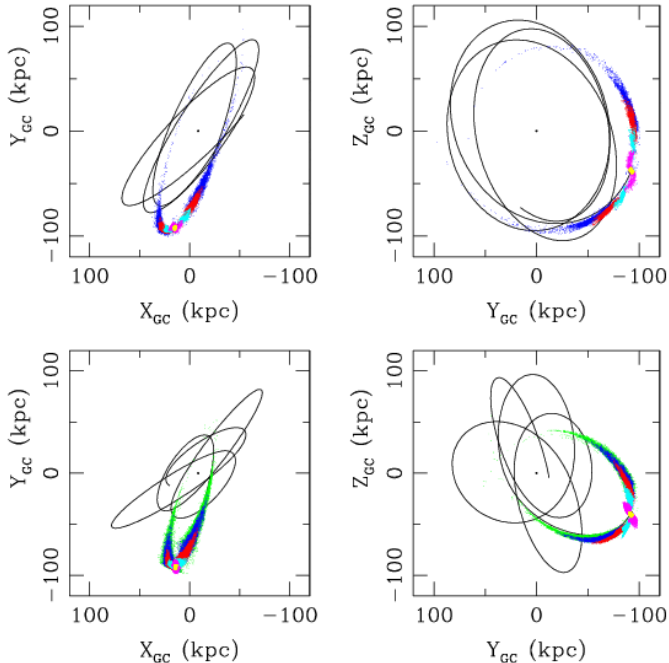


FIG. 4.— $X_{GC}-Y_{GC}$ and $Y_{GC}-Z_{GC}$ Cartesian projections for a model with a starting mass of $10^7 M_{\odot}$ in two rather benign orbits. The upper panels show the satellite in a $v_{par} = 0.8$ orbit while the lower panels show the system in a $v_{par} = 0.5$ orbit. The coloring scheme is as follows: Yellow dots mark particles that are still bound, while green, blue, red, cyan and magenta represent material that became unbound after 1,2,3,4 and 5 orbits respectively.

satellite is completely destroyed, the radial density profile of the satellite resembles an “inner King+extended population” profile that looks nearly the same for different orbital passages when viewed at the same orbital phase (uppermost panels of Figures 2, 3, 6, 8 and 9). Figure 8 demonstrates our general finding that the overall spatial and dynamical character of disrupting satellites can be maintained for long periods of time — as long as the satellite maintains a bound core but undergoes a more or less steady mass-loss-rate. This is an advantageous property of our models over the previous, more specialized N -body simulations of tidal disruption. In contrast to, for example, the findings of PP95, the specific physical satellite properties we seek in the models are not rare phenomena that we have to “catch” at special times in the life of the satellite, but rather long-lived phenomena that require no invocation of particular timing (apart from observing the system at the proper orbital phase — near apogalacticon in the case of Carina, which is a position near where satellites spend a considerable fraction of a radial period). Our dSph models also differ from those of Kuhn (1993) and Kroupa (1997) where the satellites must be observed at very specific times in their tidal evolution (namely, after total disruption or just prior to total disruption for these two references, respectively) and along specific lines of sight.

On the other hand, Figure 8 shows that while the overall character of the satellite density and velocity dispersion profiles is maintained for long periods of times, there is *some* gradual evolution in the scaling of the density profile and the magnitude of the velocity dispersion at large radii that is dependent on the amount of past disruption. Figure 8 shows the velocity dispersion profile observed today for satellites with the same initial mass (in this case $10^6 M_{\odot}$) on the same radial

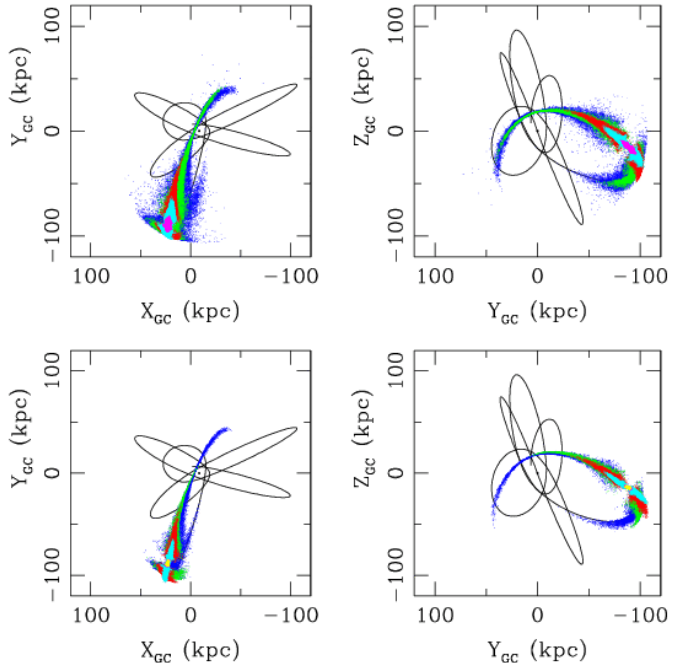


FIG. 5.— $X_{GC}-Y_{GC}$ and $Y_{GC}-Z_{GC}$ Cartesian projections for two models in rather eccentric orbits ($v_{par} = 0.3$) after five perigalacticon passages. Both models had an initial mass of $1 \times 10^7 M_{\odot}$ but the upper panels show the model with a $r_0 = 0.28$ kpc (less dense) while the lower panels show the model with a $r_0 = 0.194$ kpc (more dense). The coloring scheme is the same as in Figure 5. As may be seen, the lower density model is destroyed after five orbits (no yellow component) but the higher density model keeps a predominantly bound core.

orbit, but which have been dropped into the Galactic potential at successively earlier apogalactica. In this case, a central dip to a progressively lower central velocity dispersion is observed, while the dispersion of the debris-dominated part of the system changes with time, with slightly colder debris accumulating after the satellite has suffered more mass loss. Of course, this mass loss causes the overall density of the satellite (at all radii) to drop with time. The trend of the phenomena shown in Figure 8 thus admit yet another “free parameter” — i.e. number of orbits of tidal interaction — that one may tune, in addition to orbit shape, initial satellite mass, and satellite scale, to match the properties of any particular real satellite, such as the Carina system.

3.1.4. What is needed to match Carina?

In only one part of the systemic survey of orbit, mass, density parameter space do the simulations reproduce the general character of the observed Carina velocity dispersion profile *as well as* the general projected density distribution of Carina. The operative conditions in common among the “successful” models is a satellite that experiences intense, periodic tidal shocks at the perigalacticon of a very radial orbit, but one that also retains a bound core. Most of the models run with a $v_{par} = 0.3$ satellite orbit (orbit 2), which have peri:apogalactica of 15:103 kpc and radial periods of 1.5 Gyr, share this character (e.g., Fig. 8), as do some model satellites on the less extreme orbit 3 ($v_{par} = 0.4$).

We may summarize the results of this initial survey of parameter space to find a model that resembles Carina as follows:

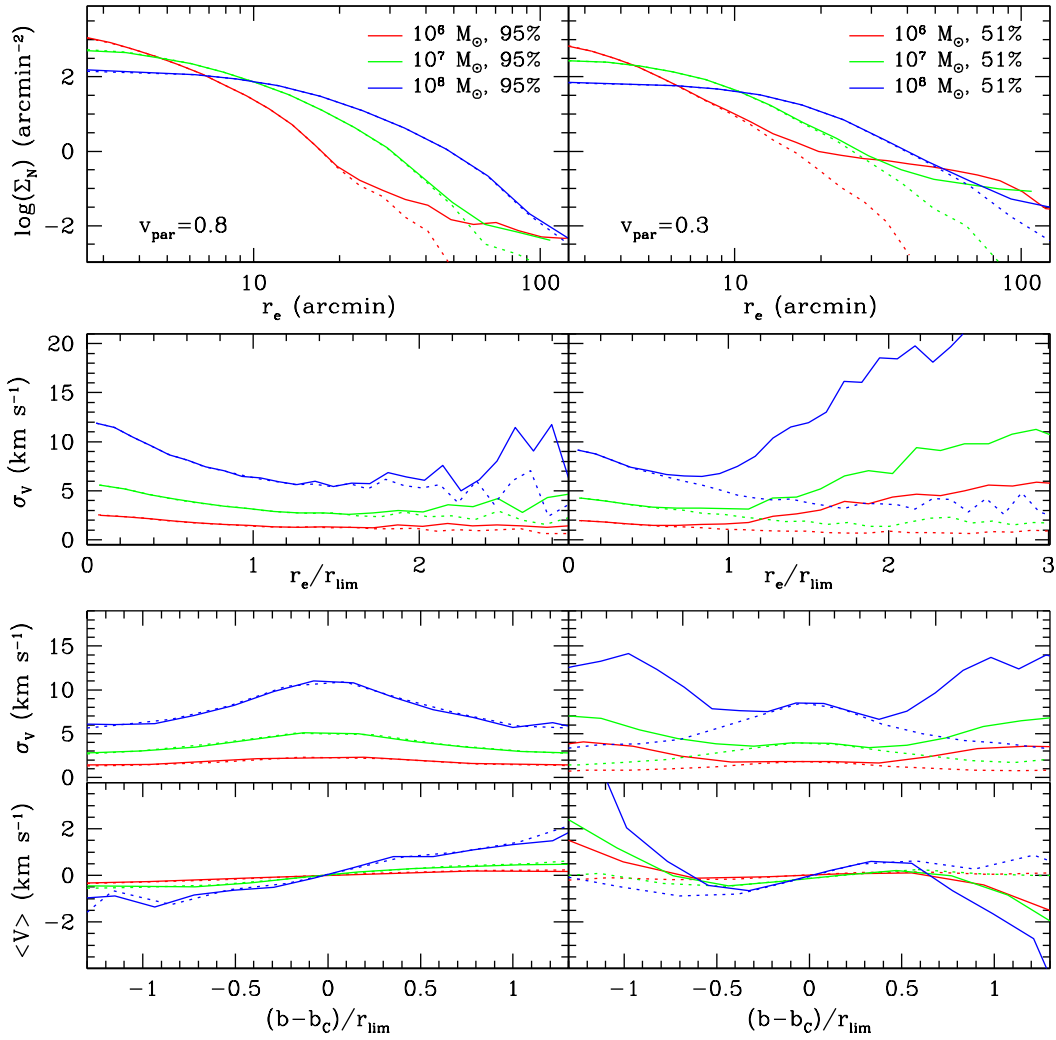


FIG. 6.— Same as Figure 3 but this time, (*left panels*) model satellites of masses 1×10^6 (red lines), 1×10^7 (green lines) and $1 \times 10^8 M_\odot$ (blue lines) with initial central density kept constant by adjusting the Plummer scale length (see text) in a rather circular ($v_{par} = 0.8$) orbit, and (*right panels*) the same model satellites but now in an eccentric orbit ($v_{par} = 0.3$). As in Figure 3, the percentage numbers represent the fraction of bound mass remaining at the end of the simulation. Solid lines represent all particles while dotted lines show the behavior of the bound particles only.

- It is possible to find MFL N -body models of disrupting satellites, constrained to the present position and radial velocity of Carina, that reproduce the general morphological character (i.e., a “inner King+extended population” radial density profile) and dynamical character (i.e., a flat/rising dispersion profile with radius) observed in the Carina system.
- The common properties of models succeeding in this way are that the satellite retains a bound central core but experiences periodic, impulsive shocks on a relatively radial (e.g., 7:1) orbit that spawns nearby clouds of unbound tidal debris. Carina resembles the system as observed near the apogalacticon of one of these orbits.
- The rise in the velocity dispersion away from the core is caused by the growing contribution of unbound debris which becomes important even well inside the projected limiting radius of the bound component. The rising dispersion profile at larger radii is due to the dominance of tidal debris there.
- Our simulations do not depend on special timing to match the general Carina properties, other than observing the system near the correct orbital phase. Thus, the results of our modeling do not hinge on particularly special circumstances other than that the satellites be on rather radial orbits.

In the next section we explore this family of models further, both to find a better match to the Carina data by fine-tuning the orbital properties, and to understand the implications of such models for the possible physical state (e.g., mass, M/L , mass-loss-rate) of the Carina system.

3.2. Fine Tuning the Models

3.2.1. Zeroing in on Carina

>From the previous general survey of single component N -body simulations we understand that orbital shape plays a critical role in producing the dynamical effects we seek to emulate in the Carina system, and that very radial orbits are preferred for a good match to the observed Carina properties. To obtain an even better match to the observations, it is worth-

TABLE 2
 MODEL PARAMETERIZATIONS^a

initial mass (M_{\odot})	Scale						
	0.045	0.090	0.194	0.280	0.350	0.418	0.550
10^6	2	(1-6)*,7-9	2-9			2*,3-9	
3×10^6	1,2*	1,2*					
10^7		(1-4)*,5-9	2*,3-9	2*,3-9		2-9	
3×10^7				2			
3.75×10^7					2		
4.5×10^7						2	
10^8		2-9	2-9			1-9	2

^a Entries give orbits run for each satellite and scale mass. Boldface entries highlight the initial parameterization used. Asterisks denote models run with multiple versions having the satellite undergo present time.

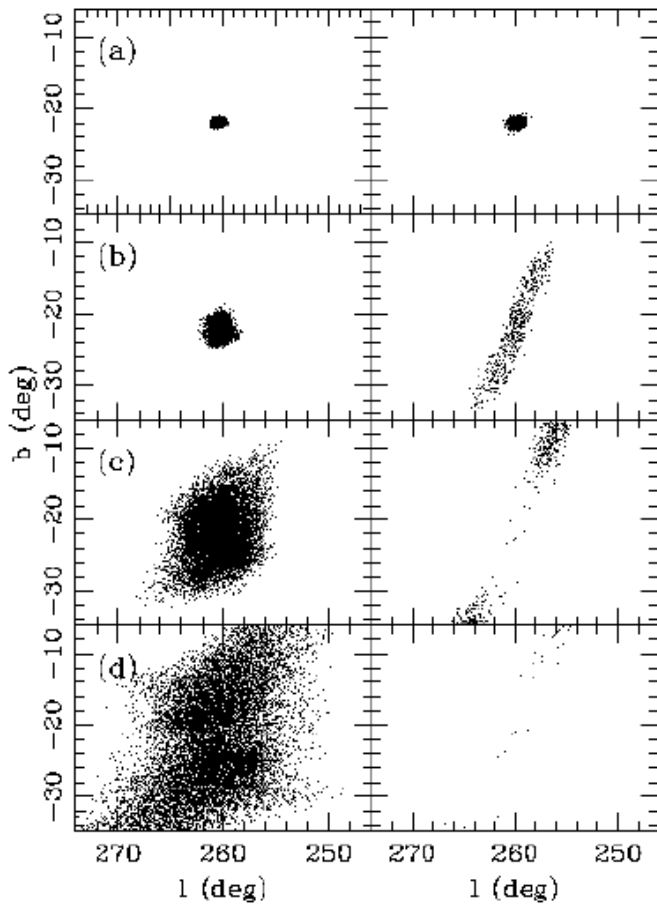


FIG. 7.— (a) Spatial distribution of bound particles for a model of $1 \times 10^7 M_{\odot}$ and $r_0 = 0.194$ kpc. Panels (b), (c) and (d) show the spatial distribution of particles lost during the last and successively previous orbits respectively (equivalent to the different colors debris shown in the other models portrayed in Figures 4 and 5). Left panels show the satellite in an eccentric ($v_{par}=0.3$) orbit while the right panels show the same satellite in rather circular ($v_{par}=0.8$) one. As may be seen, the nearby debris is dominated by particles released during the last orbit, although debris released in previous passages can linger near the center for many orbits in the case of eccentric orbits.

while investigating a finer gradation of parameter space for these radial orbit models. For now, we focus on models with satellites on orbit 2. With our single-component models this leaves as free parameters to vary: the initial satellite total mass, scale, and duration of the numerical integration (i.e., number of radial orbits). These parameters are expected to

affect the satellite and debris in certain ways for a particular orbit:

- The measured King core radius (r_{core}) and r_{lim} will obviously be influenced by the input physical scale of the satellite, r_0 .
- The central velocity dispersion of the satellite is expected to vary dimensionally as (mass/scale).
- The amount of debris is set by the mass-loss-rate and this is correlated to the density of the satellite (for a given orbit). Thus it scales as (mass/scale³). This will affect not only the relative density of the extended population to the central density of the satellite in the radial profile, but, of course, how quickly the velocity dispersion switches from being dominated by bound versus unbound debris.
- As we have seen above and in our previous studies of Sgr debris (Law et al. 2005), the velocity dispersion of tidal debris correlates with the satellite mass as long as the satellite maintains a bound core.

Guided by these rules of thumb, we attempt to vary the mass and scale of the model satellite in a way to best match the radial velocity dispersion and radial density profiles simultaneously.

First, we set the physical scale. Since we are looking for a model that matches all of the Carina properties, we start by requiring the model satellite to have a physical scale matching as closely as possible that of Carina. Considering that the size of the bound component of the model satellites does not vary significantly over their lifetime (e.g., Figure 8), we set the Plummer physical scale of our model Carina guided by the observed Carina core radius, $r_{core} = 258$ pc (Mateo 1998). Not surprisingly, King distributions fitted to satellites modeled in our initial general survey (see Appendix A) show that those with $r_0 = 0.280$ kpc yield the closest match to the Carina density profile — i.e., those for which r_0 is similar to Carina's r_{core} .⁸

Once the physical scale is set, we seek a model that is capable of reproducing the observed *central* velocity dispersion of Carina (6.97 ± 0.65 km s⁻¹, from Muñoz et al. 2006a). Since this varies as (mass/scale) and the scale of the model is already

⁸ While r_{core} radius and the Plummer length scale of a given density distribution are not strictly equivalent, their ratio is of order unity for low concentration systems like dSphs.

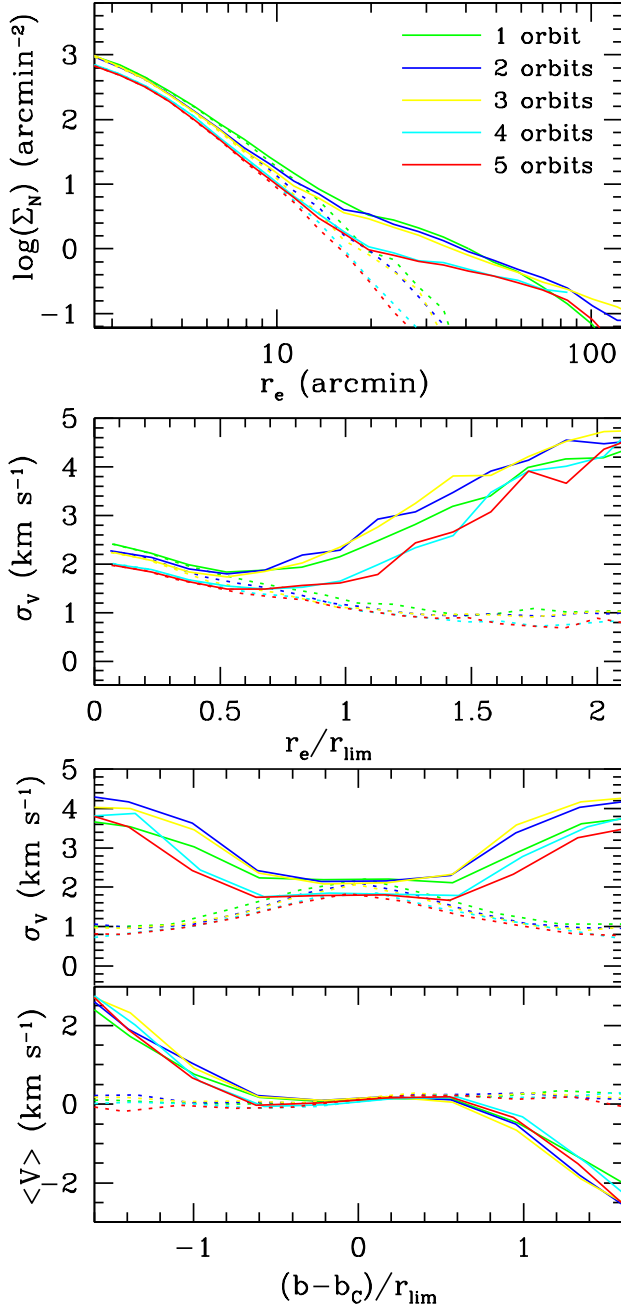


FIG. 8.— The evolution of the density, velocity dispersion and mean velocity profiles over five orbits for one of the low mass, medium density, radial orbit models showing the general properties observed in Carina. This shows that satellites can retain the general character of a rising velocity dispersion over many orbits, but the asymptotic dispersion value is a function of the amount of past disruption.

set, that leaves us with the initial mass as the pertinent variable. But by varying the initial mass we are also simultaneously changing the initial density of the model and that drives the mass loss rate, which, in turn, affects the shape of the velocity dispersion profile as well as the current bound mass of the satellite; these observational constraints *each* tightly and independently constrain the choice of mass. Nevertheless, a model reasonably matching *all* of these constraints can be

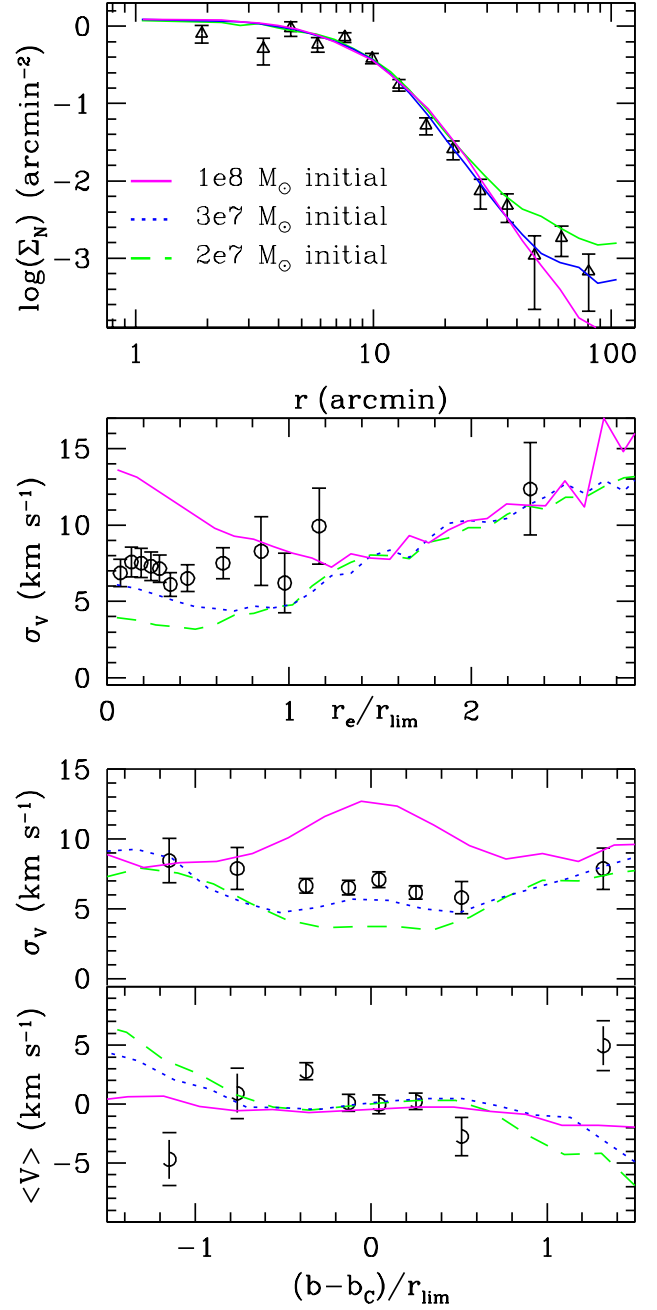


FIG. 9.— Three models with an initial physical scale of $r_0 = 0.280$ kpc, chosen to yield present satellite sizes comparable to that of the luminous component of Carina (see text for details). Three different initial masses of 2.3 and $10 \times 10^7 M_\odot$ are shown to explore the resulting number density, velocity dispersion and mean velocity profiles. Data from Muñoz et al. (2006a) are shown for comparison as open symbols with error bars.

found.⁹ For example, Figure 9 shows the velocity dispersion, projected mean velocity and density profiles for satellites in a $v_{par} = 0.3$ orbit with initial masses of 2×10^7 , 3×10^7 and $1 \times 10^8 M_\odot$, after 5 orbits. The lower and higher mass models

⁹ The fact that all of these constraints can be simultaneously satisfied lends considerable weight to the viability of the single component models; after all, were they an incorrect description of the physical state of Carina, it is easy to imagine our models having difficulty satisfying all observable constraints with the limited number of free parameters.

yield current central velocity dispersions that are too low and high compared to Carina respectively, while the intermediate mass model gives the closest match. This intermediate mass model provides a better-matching density distribution as well.

While Figure 9 demonstrates that of the three models shown the $3 \times 10^7 M_\odot$ model provides the closest match to the shape of the velocity dispersion *profile*, its values are still systematically low compared with the data. Further fine tuning of the model Carina thus requires an overall increase of the velocity dispersion. We achieve this by increasing the initial mass of the model while at the same time making the orbit slightly more eccentric to keep a similar mass loss rate. The net effect is a model that yields the right central velocity dispersion while at the same time providing a good match to the shape of the velocity dispersion and the number density profiles (those shown in Figure 10).

Finally, we note that models initially run and presented so far were designed to have an orbital pole of $(l, b) = (159.3, -12.9)^\circ$. But when we eventually collected spectroscopic data at large radius (presented in Muñoz et al. 2006a), we found that these models were actually yielding the opposite mean velocity trend from that being found in Carina (Fig. 2). To fix this difference with our completed simulations, in the end we re-computed our best matching models by placing the satellites on orbits with the polar antipode of $(l, b) = (339.3, 12.9)^\circ$ to obtain the correct velocity trend.

Tables 3 and 4 give the parameters for two models (502G and 502I) that yield close matches to the data. As may be seen, these “best matching” models to the Carina structure and dynamics have initial masses of 3.6 and $3.8 \times 10^7 M_\odot$, but have evolved after five orbits to present masses of $\sim 1.9 \times 10^7 M_\odot$. Interestingly, these final masses are comparable to the current mass of Carina derived using the core-fitting method (Mateo et al. 1993; Muñoz et al. 2006a; see §3.2.2). Figure 10 compares the final state of these simulations against the data for Carina. In the top panels, we compare the number density profiles. In the middle pairs of panels we compare the velocity dispersion profiles both as a function of angular distance from the center of Carina and as a function of Galactic latitude respectively, and in the bottom panels we compare the mean velocity trend of the satellite in Galactic Standard of Rest velocities. For both simulations 502G and 502I, the models lie within $1\text{-}\sigma$ of the data for almost all positions in the dSph for *all four* of the observational trends shown.

3.2.2. Mass-to-light ratios

Tables 3 and 4 also give for the different models the evolution of the satellite from its initial conditions at each apogalacticon and at the final state, with the distance, best fitting central King profile parameters (see Appendix A), fractional bound mass remaining, and central velocity dispersion given. As may be seen, the actual King profile radii of the satellites remain relatively constant through time. However, the central velocity dispersion is seen to drop as the satellite loses bound mass, closely tracking the instantaneous mass — as expected if the steady state virial theorem remains a good approximation in the face of relatively modest mass loss rates.

If we desire the M/L of the satellite to remain constant in time (i.e., dark matter and luminous matter are lost in equal proportion for MFL models), then the central surface brightness of the satellite must evolve scaled to σ^2 . To demonstrate that this actually happens, we also give for each apogalacticon time stamp in Tables 3 and 4 a measurement of the

global M/L as inferred using the standard core-fitting technique (Illingworth 1976) applied with the velocity dispersion and core radius measured at that point in the simulation:

$$(M/L)_{\text{tot}} = \frac{166.5 R_{c,g} \mu}{\beta L_{\text{tot},V}} \quad (3)$$

Application of this equation requires calibration of the models by the actual central surface brightness in order to “paint” an appropriate fraction of the particles as luminous. For the final time stamp of the models, which are intended to represent the present Carina dSph, we simply adopt the observed luminosity of Carina of $4.3 \times 10^5 L_\odot$ from Mateo (1998). Once this is done, we can determine the scaling from particles to luminosity by the ratio of the actual luminosity to the total number of particles in the final time step of the model. This scaling allows us to track the *measured* M/L of the satellite as determined through core-fitting backwards over time (e.g., the ninth column in Tables 3 and 4). But because we are assuming MFL, we can of course independently assess what the *actual* M/L of the bound system is (which is constant by design) by the fact that we know what the bound mass is at the last stage of the simulation and we are assuming the satellite has currently the luminosity of Carina. Tables 3 and 4 shows that the M/L derived by core-fitting reasonably matches the actual M/L of the model throughout its evolution. We have found that this condition breaks down only when the satellite reaches near complete dissolution, as previously reported by Kroupa (1997). The stability of the observed M/L with time is another convenient feature of our models that frees us from concerns about special timing requirements to match models to data. Moreover, it is not a forced condition, but one that arises naturally in our models.

3.2.3. Comparison to Proper Motion-Derived Orbit

The orbital parameters of those models that give the best match to the observed Carina properties (Tables 3 and 4, Figure 10), are in very good agreement with the one previous attempt to determine the orbit of Carina directly. Piatek et al. (2003) measured the proper motion of Carina using HST imaging and found that the dSph must currently be near apogalacticon, and they derive the best estimate for apo- and perigalactica at, respectively, 102 and 20 kpc; this is in very good agreement with our results of 103 and 15 kpc. Piatek et al. (2003) also give an estimate for the orbital period of 1.4 Gyr; again, this matches well our derived period of 1.5 Gyr. Although their study does not find Carina in a polar orbit (the inclination of their derived orbit with respect to the Galactic plane is 39°), the 95% confidence interval for their derived inclination is so wide ($23^\circ, 102^\circ$) that it includes a polar orbit such as we derived here¹⁰.

In summary, our “fine tuning” procedures have allowed us to find MFL, tidal disrupting satellite models that quite successfully fit the prime observational properties of Carina: the velocity, velocity dispersion and radial density profiles. Moreover, along with other properties that arise naturally, such as the close and correct tracking of the instantaneous central M/L , these model properties (1) do not require special conditions (e.g., particular viewing perspectives, critical evolutionary states) to be observed, (2) have long term stability over

¹⁰ Our own derived orbital inclination (§2) is based solely on the general orientation of the extended Carina population (Fig. 1; see also Fig. 3) and this estimate itself is likely subject to some 10° uncertainty.

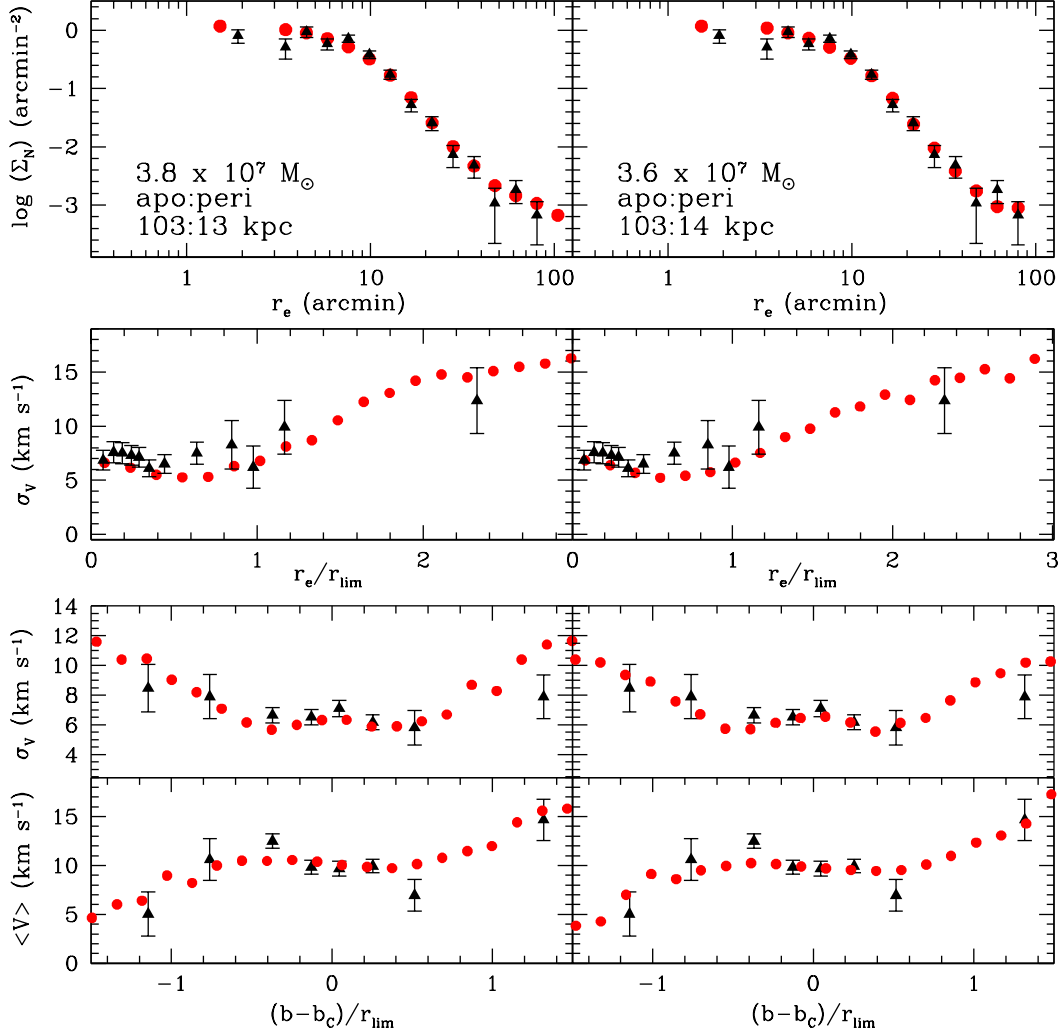


FIG. 10.— From top to bottom: Number density profiles, velocity dispersion versus radial distance, velocity dispersion as a function of major axis, and mean RV trend (with velocities in the Galactic Standard of Rest frame) for our two best matching models. Model 502I is shown by the left panels and model 502G by the right ones. The data for Carina from Muñoz et al. (2006a) are shown as solid triangles.

TABLE 3
PROPERTIES OF MODEL 502G^a

orbit	D (kpc)	r_{core} (pc) ^b	r_{lim} (pc) ^b	R_{tidal} (pc) ^c	σ_v (km s ⁻¹) ^d	M_{bound} ($10^7 M_\odot$)	M_{bound}/M_0	$(M/L)_{cf}$ ((M/L) $_\odot$) ^e	$(M/L)_m$ ((M/L) $_\odot$) ^f
0	104	230	725	550	8.73	3.60	1.00	38	45
1	96	220	710	535	8.48	3.26	0.91	38	45
2	97	220	760	505	7.96	2.77	0.77	39	45
3	106	225	770	490	7.60	2.48	0.69	41	45
4	97	235	700	470	7.22	2.23	0.62	43	45
5	101	250	815	450	6.83	1.94	0.54	47	45
Carina ^g	101	258	846		6.97	1.76		41	

the life of the satellite, and (3) do not require the invocation of extra free parameters beyond initial satellite mass, scale, and orbital shape.

3.2.4. Tidally Induced Ellipticity?

Despite being a good match for most of the structural and kinematical properties of Carina, the only shortfall of our models that we have found is that they fail to match Carina's observed ellipticity (0.33, Mateo 1998); rather, in general the

models maintain bound components that are nearly spherical. Obviously, elongation of the model satellites is observed over very large scales, when tidal debris starts to organize into tidal tails, but not over radii where ellipticity is seen in the dSphs.¹¹

While spherical cores are a general result for those models

¹¹ The orientation of the nascent tails in the simulations agrees with the observed intrinsic elongation of Carina, but of course the orbital poles for the simulations were chosen assuming that the major axis of Carina lies along its orbital path (§2).

TABLE 4
 PROPERTIES OF MODEL 5021^a

orbit	D (kpc)	r_{core} (pc) ^b	r_{lim} (pc) ^b	R_{tidal} (pc) ^c	σ_v (km s ⁻¹) ^d	M_{bound} (10 ⁷ M _⊙)	M_{bound}/M_0	$(M/L)_{cf}$ ((M/L) _⊙) ^e	$(M/L)_m$ ((M/L) _⊙) ^f
0	105	250	900	500	9.00	3.80	1.00	40	43
1	97	230	740	485	8.70	3.42	0.90	38	43
2	97	250	770	455	7.89	2.83	0.74	41	43
3	106	230	715	435	7.59	2.50	0.66	39	43
4	97	230	760	420	7.16	2.21	0.58	40	43
5	101	235	850	395	6.60	1.85	0.49	41	43
Carina ^g	101	258	846		6.97	1.76		41	

^a Run in an orbit with R_{apo}/R_{peri} of 101/15 kpc.

^b Core and King radius from best fitting to bound population.

^c Tidal radius from equation (2) (Oh et al. 1992).

^d Central projected velocity dispersion.

^e Global Mass to Light Ratio from Core-Fitting technique applied to the model’s structural parameters.

^f Global Mass to Light Ratio from the known bound mass in the model. This value is constant over time by design.

^g D , r_{core} and r_{lim} from Mateo (1998). σ_v and $(M/L)_{cf}$ from Muñoz et al. 2006a.

that retain a significant fraction ($> 10\%$) of their initial mass as bound, satellites with a bound core but having the observed ellipticity and position angle of Carina are obtained only when $\sim 5\%$ or less of the initial mass remains bound. Figure 11 (upper panel) shows a contour map of the density distribution for a model that is near complete destruction. The elongated appearance of the satellite is clear. Interestingly, when they are near destruction, these satellites exhibit a kinematical behavior similar to that described by Kroupa (1997) — that is, their central velocity dispersions are significantly inflated along with an associated artificial increase in the inferred central mass density and total mass. However, in these cases, the satellites no longer provide a good simultaneous match to the density and velocity dispersion profiles of Carina, as Figure 12 shows, due, partly, to a sudden and significant inflation in the satellite size (by up to an order of magnitude) with respect to its starting scale length. We conclude, therefore, that if our MFL models provide the correct explanation for the structure and dynamics of Carina, the observed ellipticity in this satellite is not likely tidally induced (see §4.2), and is probably related to the initial shape of the satellite.

4. DISCUSSION

Our work here has demonstrated several important features of tidal disruption and the dark matter content of dSphs in general, and of the Carina dSph in particular. These results are at odds with some commonly held perceptions regarding the observable effects of tidal disruption. These perceptions have partly been driven by extrapolating the results of PP95 and OLA95 beyond the specific cases actually explored in those papers. We use our analysis of tidally disrupting N -body satellites to readdress eight statements commonly made about dSphs and tidal disruption that we believe are either incorrect, or at least are overly simplistic.

4.1. *Misperception 1: Lack of Rotation Signatures Means Tidal Disruption Is Not Happening*

Current RV surveys of Galactic dSphs extend now to the outskirts of these systems (as defined by the distribution of their luminous matter) and this provides new constraints useful for checking the dynamics of tidally disrupting N -body simulations. PP95 stated that the most useful result from their N -body simulations is the identification of tidally induced rotation along the major axis of the system as a signature of tidal disruption. Subsequently, this has become perhaps one

the most widely used criteria to assess whether tidal stripping is affecting particular dSph systems.

To date, kinematical surveys of most dSphs have found little evidence for significant rotation. This lack of a clear rotational signature has thus lead to the conclusion that tidal stripping of Galactic dSphs is for the most part unimportant (e.g., Kleyna et al. 2001; Koch et al. 2007a,b). However, even careful examination of the PP95 results indicates that lack of rotation signatures within current RV surveys is not necessarily indicative of the importance (or lack thereof) of Galactic tides. PP95 found significant rotation along the major axis of their model satellites *only when the satellites were near perigalacticon of their eccentric orbits and when the host galaxy’s mass distribution was modeled as a point mass*. But PP95 also noted that when the Galactic halo was modeled by a more realistic potential, this apparent rotation became less pronounced in their models and was only observed over large spatial scales (this point was also made by OLA95). Perhaps most relevant to the typical Galactic satellites, PP95 saw that the rotation signal effectively disappears as the satellites move to apogalacticon, and this is an orbital phase near where satellites are most likely to be observed. Our more comprehensive exploration of satellite parameter space and modeling in a more realistic MW potential also indicates that tidally induced rotation is not always a good discriminator of tidal disruption. As discussed in §3.1.2, detectable levels of induced rotation along the major axis is only observed over scales larger than approximately r_{lim} of the model satellites, whereas most current RV surveys are confined to regions interior to these radii.

Thus, because tidally induced rotation can be completely unobservable within the current spatial limits of most dSph RV surveys for satellites at typical points in their orbits, this test is not reliable for *ruling out* tidal disruption. Eventually, when large enough radii can be probed dynamically, this kind of test may be more appropriate; this is the case for Carina where RV members have been detected to at least $4.5r_{lim}$ and rotation along its major axis is observed beyond its r_{lim} .

However, an additional complication to using this “rotation” test over large angular scales is that even if a satellite is completely bound, eventually the varying projection of the satellite bulk motion on the radial velocity can produce an apparent “shearing” trend similar to the one caused by tidal effects. If the mean velocity as a function of position can be ascertained with great enough precision, it may be possible to discriminate the more uniform trend produced by projection

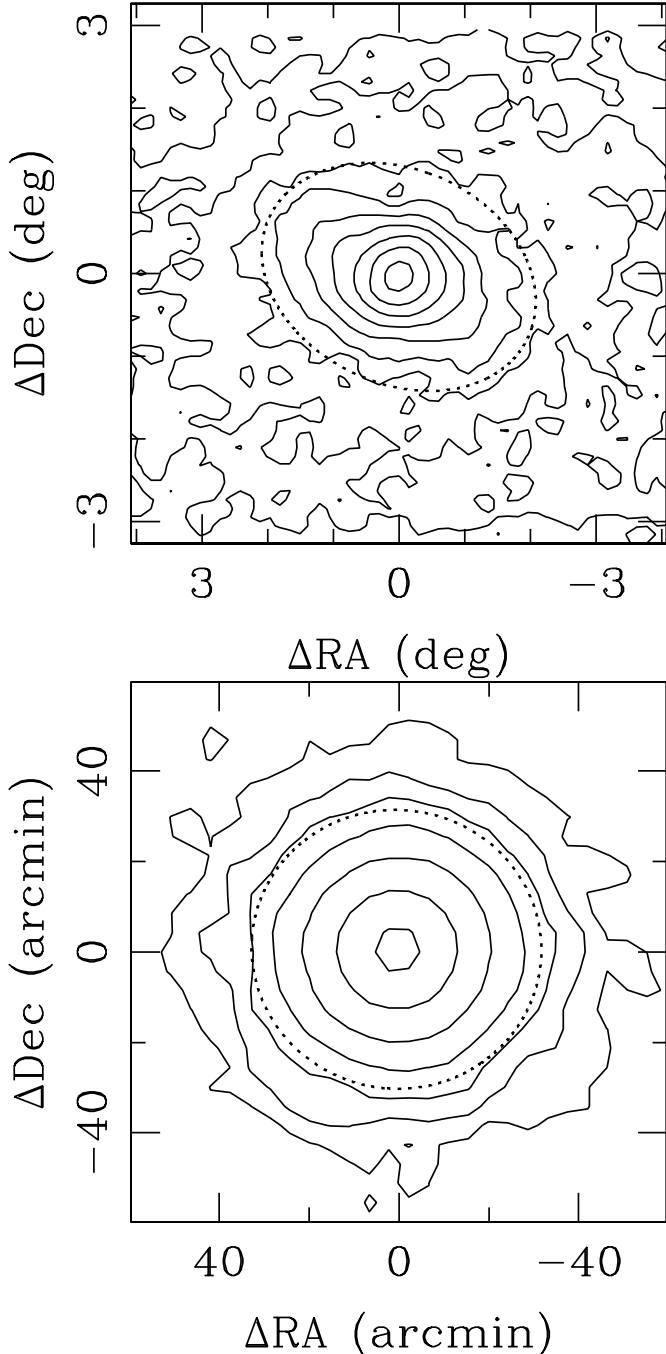


FIG. 11.— *Upper panel*: Isodensity contours for a model satellite right before it becomes completely unbound (5 % of initial mass still bound). As the satellite is on the verge of being destroyed the bound component of the satellite enlarges and elongates. *Lower panel*: Isodensity contours for one of the Carina’s best fitting models (502I). Only particles within two King radii, marked by the dotted ellipse) have been considered to mimick the surface brightness limitations of current photometric surveys. The contours have been plotted roughly evenly spaced in radius. The density contours show a remarkably regular structure, with no tail-like structures visible despite the satellite losing nearly half its initial mass.

from the more *S*-shaped trend seen in many tidal disruption models, but the differences are subtle.

4.2. Misperception 2: Tidally Disrupting Satellites Have Pronounced Ellipticities

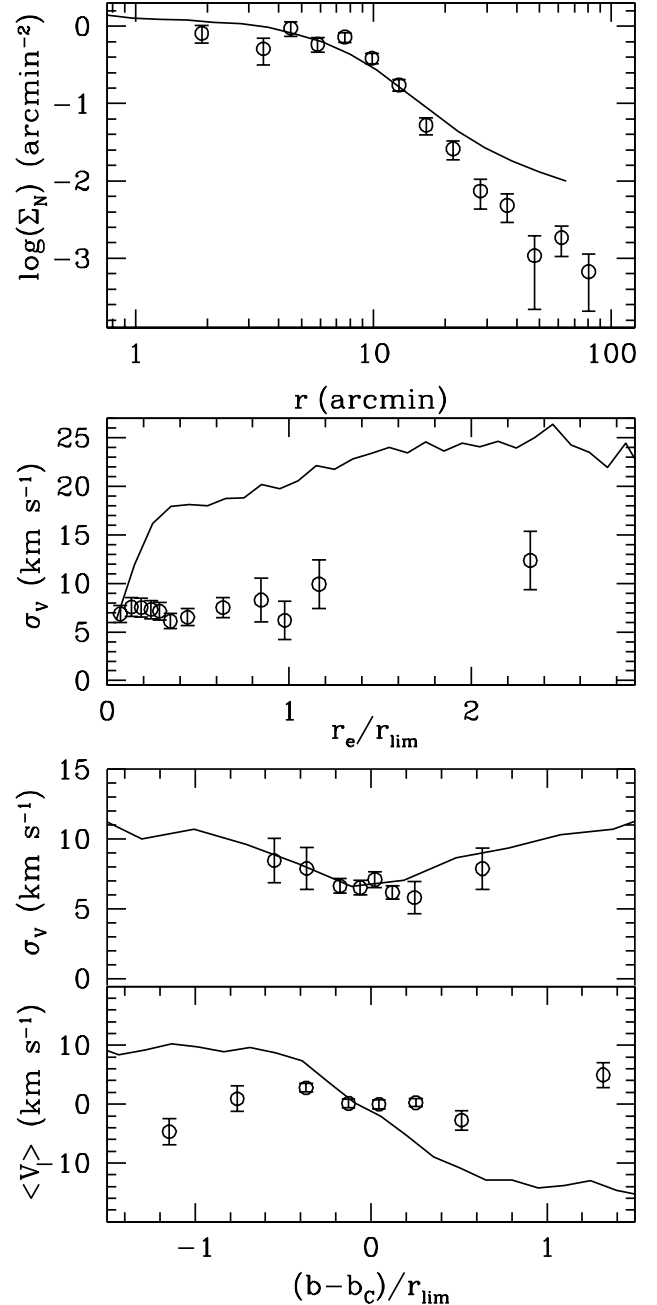


FIG. 12.— Number density, velocity dispersion and mean RV trends for the satellite shown in the upper panel of Figure 11. Data points are overplotted for comparison as open symbols. The model satellite has become significantly enlarged compared to its initial size, and it has been scaled down by a factor of four to compare to the data. While the velocity dispersion along the major axis of the model seems to provide a good match to the data (after being scaled down), the rest of the observed properties of Carina are not well match by the model (even when scaled down).

An interesting result from our general survey is that for models that retain a bound core with more than $\sim 10\%$ of the initial mass, the bound component of our satellites always remain spherical, with no perceptible, tidally induced elongation. Figure 11 (lower panel) demonstrates this situation: Here, we show the contours of the projected number density of one of our best matching Carina models only using particles within two r_{lim} . Even though some debris is projected

within r_{lim} , the overall azimuthal satellite density distribution is dominated by the still bound material and, as is readily obvious, the contours show no substructure or clumping and the satellite remains fairly round and regular.

This lack of tidal elongation in our model seems to be, in principle, at odds with the findings of PP95 (see their Figure 5). These authors found their simulated satellites enlarged and presented projected ellipticities as high as 0.7, which PP95 ascribed solely to the effects of Galactic tides. But a careful comparison between our simulations and PP95's indicates that there is no actual disagreement between our models and theirs, only on the respective interpretation of the models. As in the case of apparent rotation (§4.1), the tidally induced ellipticity observed by PP95 pertains to the specific case of a satellite being observed just before it becomes completely destroyed and when the MW has been modeled as a point mass. As presented in §3.2.4, model satellites in our survey that are near complete disruption, with only a small fraction of the initial mass still bound (typically 5% or less), also “puff up” relative to their original size and they also typically elongate along their major axis (Figure 11, upper panel).

That none of our surviving model satellites present tidal elongation within their tidal limits suggests then that perhaps the ellipticity observed in some Galactic dSphs corresponds to a process other than tidal stripping, even if the satellites are currently experiencing mass loss. For example, if dSph morphologies are the result of tidal stirring of disky dwarf irregular galaxies (Mayer et al. 2001a,b, 2007) the triaxiality of the progenitor system may be preserved for some time. This might also explain why, in the cases where proper motions have been measured, there is not always a correlation between the observed position angle of the satellites and the direction of their orbit (e.g., Piatek et al. 2003, 2005, 2006).

Once again, our more systematic exploration of parameter space illustrates that one must be careful not to extrapolate the results of the earlier, more specific models and expect effects that are not necessarily general in nature or that are actually beyond the range or sensitivity of current surveys. In this case, the elongation reported by PP95 and in our simulations is from the nascent tidal tails, and therefore, to see the effect, one must look at radii where the debris makes a substantial relative contribution to the bound particles (e.g., Fig. 13). This is beyond the typical surface brightness limits and/or radii of most previous photometric studies of dSphs (other than our own — e.g., Majewski et al. 2003, Muñoz et al. 2006a, Sohn et al. 2007).

4.3. Misperception 3: No Detected Tidal Tails Means No Tidal Disruption

One of the most unmistakable signatures of a system undergoing tidal stripping is the development of debris tails which, in general, closely trace the orbit of the satellite (e.g., Johnston 1998). Perhaps the most striking examples in the MW system of satellites exhibiting tidal tails are the Sagittarius dSph (Majewski et al. 2003) and the Palomar 5 globular cluster (Odenkirchen et al. 2003; Grillmair & Dionatos 2006a). Several other recently found stellar streams have no clear progenitor but have been traced for tens of degrees on the sky (e.g., Grillmair & Dionatos 2006b; Grillmair 2006; Belokurov et al. 2007). Several photometric studies have been carried out over the years to look for unmistakable evidence of tail-like features around other Galactic dSphs, but with the possible exception of Carina (Muñoz et al. 2006a), such evidence has been lacking. This absence of detectable

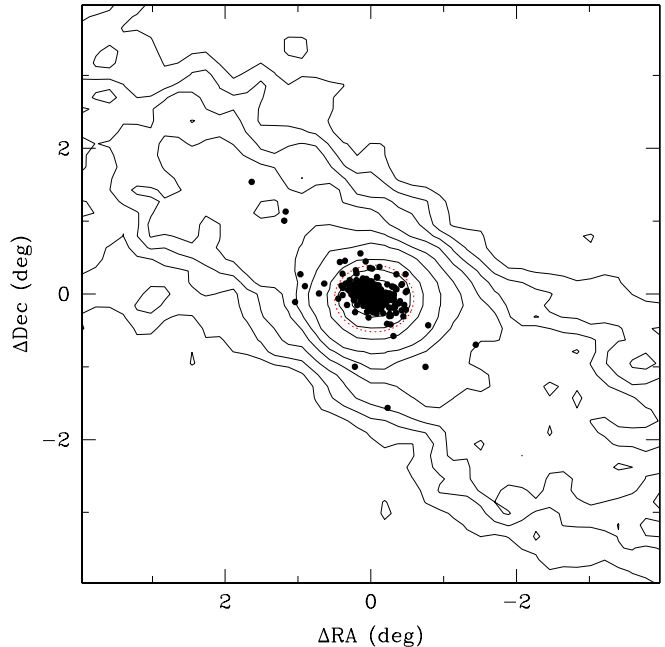


FIG. 13.— Isodensity contours for the same model shown in the lower panel of Figure 11, but when particles over a four degree radius are considered. Again, the contours have been plotted roughly evenly spaced in radius along the minor axis. The contour levels shown (from faintest to brightest up to r_{lim}) correspond to the following surface brightness levels: 35.5, 34.9, 34.6, 34.2, 33.8, 33.3, 32.0 and 30.4 mag arcsec $^{-1}$ (assuming the central surface brightness of the model satellite is $\Sigma_0=25.5$ mag arcsec $^{-1}$ in the V-band). This time, the development of tidal tails is clearly observed, but over scales much larger than the King limiting radius. To illustrate how far out one needs to go to detect clear tidal tails, current Carina RV members have been over-plotted (as solid circles) for comparison.

tail-like structural perturbations at large radii, especially when combined with a lack of the (inappropriately) expected rotation signature of PP95, has often prompted the conclusion that Galactic tides are unimportant for most dSphs (e.g., Walcher et al. 2003; Coleman, Da Costa, & Bland-Hawthorn 2005; Segall et al. 2007). However, we can use the results of our extensive N -body simulation survey to investigate the feasibility of actually detecting tidal tails around satellites undergoing tidal disruption.

To clarify the expectations of finding tidal tails we simulate “observations” of our N -body models (where we know with certainty that tidal tails are present). If one assumes that the central surface brightness of our best matching models (502I and 502G) corresponds to the observed current value for Carina ($\Sigma_0=25.5$ mag arcsec $^{-1}$ in the V-band, Mateo 1998), then the surface brightness of their density at r_{lim} would be $\Sigma \geq 31$ mag arcmin $^{-1}$, which is beyond the sensitivity of typical photometric methods used to explore the surface brightness distribution of dSphs (see Majewski et al. 2005 for detailed comparisons of these methods). Indeed, in their exploration of the formation of a MW-like galaxy halo by Λ -CDM infall of satellites, Bullock & Johnston (2005) found most of their resulting debris streams to be fainter than 30 mag arcsec $^{-2}$, and K. V. Johnston et al. (in preparation) predict there to be only one stream brighter than this on average. The fact that our own surveys (e.g., Majewski et al. 2000, et. seq.) can probe these and the even fainter surface brightnesses of tidal tails is because of the highly tuned selection for dSph giant stars, which yields much higher signal-to-background sensitivity in the very diffuse parts of the dSph systems. Fig-

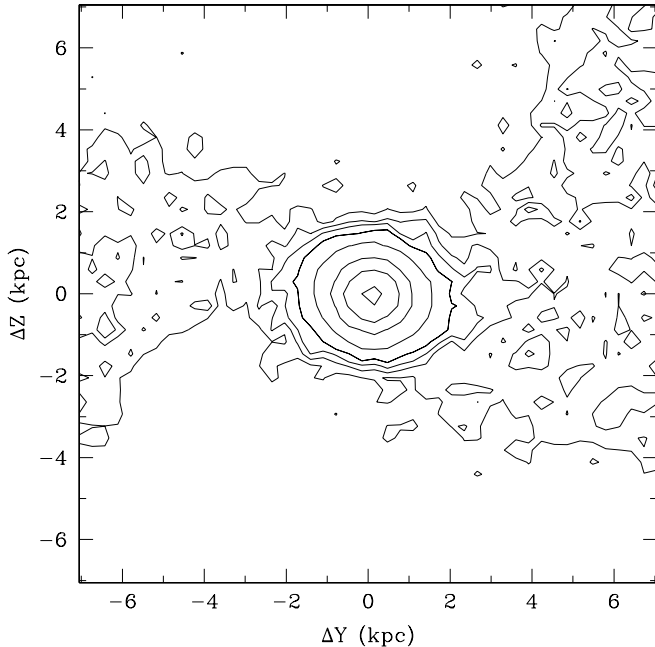


FIG. 14.— Isodensity contours for the same model and particles shown in Figure 13, but this time from a line of sight nearly perpendicular to the plane of the orbit. As it can be seen, the expected, tidally induced S-shape is barely discernible.

ure 11 (lower panel) shows that “observations” of one of our best matching Carina simulations (model 502I), to a surface brightness comparable to those of most current dSph photometric surveys would not have detected the presence of tidal tails around the model satellite.

Figure 13 expands by a factor of four the spatial scale of the density contours shown in the bottom panel of Figure 11 and includes even lower surface brightness features to the point where tidal tails are now visible (the dotted line delineates r_{lim} for this model, a radius that is well within the regions where there are tails). This figure demonstrates another challenge that photometric searches for tidal tails face: the debris around the bound core of the dSph does not organize into coherent tails immediately outside r_{lim} but the presence of tidal tails is only evident over physical scales much larger than this. Therefore, much larger systematic photometric surveys to very low detection thresholds are needed to detect unmistakably obvious tidal tails from real dSphs. On the other hand, unbound tidal debris *does* collect more or less radially symmetrically surround the dSph just beyond the tidal radius, and it is the presence of *this* “extended population” structure in the density profiles of satellites that is the more obvious, and more likely to be detected, expected photometric signature of tidal disruption. As pointed out in Section 1.1, most of the classical MW dSph satellites do exhibit this very feature in their density profiles.

4.4. Misperception 4: No S-shape Morphology Means no Tidal Disruption

Another common expectation for tidally disrupting systems related to the presence of tidal tails is the detection of stellar density contours that become progressively more elliptical with radius along with a variation of their position angles, which together result in the typical S-shape morphology associated with tidally stripped systems (e.g., PP95; Combes, Leon, & Meylan 1999;

Choi, Guhathakurta, & Johnston 2002). Examples of these morphologies have been detected in Local Group systems already proven to be disrupting, such as the M31 satellite NGC 205 (Choi, Guhathakurta, & Johnston 2002) and the Galactic globular cluster Palomar 5 (Odenkirchen et al. 2003).¹² Thus, given the apparent connection between S-shaped morphologies and tidal disruption, one might be tempted to use the lack of detection of this morphology to argue that a system has not undergone tidal interaction with our Galaxy. However, closer examination of cases where this S-shape morphology has been detected shows that usually, with the clear exception of Ursa Minor (discussed further below), the isophotal twisting occurs over physical scales larger than r_{lim} .

In addition, previous simulations (e.g. Combes, Leon, & Meylan 1999) as well as our own presented here demonstrate that, depending on the orientation of the satellite and its tails to our line of sight, this S-shape morphology may not be seen at all. Our best matching models for Carina demonstrate this situation. In Figure 13, where the tidal tails of the satellite are clearly seen, no classical S-shape is observed. In this case, the lack of detection is readily explained by the fact that this isophotal twisting occurs *in the plane of the orbit*, and, given the Galactocentric distance of Carina, which like most of the classical Galactic dSphs, is large (> 60 kpc for most cases), the projection of the orbit on the sky is not favorable for observing this morphological feature (i.e., the Sun lies relatively close to the orbital plane for distant Galactic satellites). Moreover, even if viewed in the correct orientation, the S-shape might be very subtle. Figure 14 shows the density contours for the same model and particles shown in Figure 13, but this time from a line of sight nearly perpendicular to the plane of the orbit (e.g., projected onto the Galactic $Y_{GC} - Z_{GC}$ plane). Even in this preferred orientation for observing the S-shape it is barely visible.

The case of Ursa Minor, which shows an S-shape morphology (Palma et al. 2003) but where the reported S-shape is seen well inside its r_{lim} , is thus unique and intriguing. This dSph is at a heliocentric distance of 66 kpc (Mateo 1998), and so it is unlikely that its orbital projection on the sky is favorable for viewing the S-shape, regardless of the shape of the orbit. Moreover, even if this were the case, we would expect to see isophotal twisting over scales larger than r_{lim} . In this particular case, the S-shape may be a coincidence, with the isophote bending the result of other physical effects at work to produce internal substructure. For example, the well-known secondary peak in the 2D stellar density distribution of Ursa Minor, displaced ~ 300 pc from its center, and shown to be dynamically cold by Kleyna et al. (2003), could potentially result in isopleths that just happen to mimic the S-shape twisting even if they are not of tidal origin, at least in the classical way.

4.5. Misperception 5: Flat/Rising Velocity Dispersion Profiles Require Extended Dark Halos

Most current RV surveys of dSph satellites yield velocity dispersion profiles that are more or less flat or rising all the way to the r_{lim} of the system. Recently, these velocity dispersion trends have been attributed to non-MFL, multi-component mass distributions in dSphs, with perhaps some possible additional contribution from

¹² Other systems, like the And I (McConnachie & Irwin 2006) and Ursa Minor dSphs (Palma et al. 2003) show this S-shape morphology, but in these cases, the presence of this feature has been adopted as one of the arguments that these dSphs are tidally disrupting.

velocity anisotropy (e.g., Łokas 2002; Kleyna et al. 2002; Łokas, Mamon & Prada 2005; Mashchenko et al. 2005, 2006; Walker et al. 2006a; Koch et al. 2007a,b). These multi-component models yield both total dSph masses that are up to an order of magnitude higher than those obtained by traditional core fitting techniques, as well as physical scales much larger than those of the observed light distribution, suggesting that dSphs are currently surrounded by extended dark matter halos. In some cases the derived satellite total masses approach the $10^9 - 10^{10} M_{\odot}$ range (Łokas 2002; Mashchenko et al. 2005, 2006; Read et al. 2006b).

However, our analysis of dSph properties within the context of MFL, tidally disrupting admits a workable alternative interpretation of the velocity dispersion profiles of dSph galaxies. We summarize our results with respect to the behavior of the velocity dispersion profile as follows:

- The most important observable dynamical effect of Galactic tides is to inflate the velocity dispersion at large radii and to produce a velocity dispersion profile that can go from slowly declining to flat or even rising depending on the amount of tidal debris released and disruption history of the satellite.
- The central velocity dispersion of systems that retain a bound core remains unaffected by tides, which means that its value is a good reflection of the underlying bound mass of the satellite, even when substantial tidal stripping may be ongoing.
- Completely flat velocity dispersion profiles are, in general, only achieved when the satellite has become completely unbound. The size of the velocity dispersion is driven by a complex combination of the initial satellite mass, density, orbit and number of prior orbital passages.
- The inflation of the velocity dispersion as a function of radial distance is not necessarily an effect of “cylindrically-averaged” (i.e., azimuthally averaged) dispersions as suggested by Read et al. (2006a). Intrinsic inflation is observed even when the velocity dispersion is studied along the major axis (see Figures 3 and 6).
- Completely or mostly bound systems show velocity dispersion profiles that peak at the center and decrease with radius.

Thus, there are at least two viable explanations for the flat/rising velocity dispersion profiles of dSph galaxies. However, beyond just explaining the velocity dispersion profiles, our MFL tidal disruption models are the first models that try comprehensively to match *all* presently observed general features of dSphs (except ellipticity; see §3.2.4), and that satisfy all specific constraints of the presently best-studied dSph in particular. No multi-component, tidal-stripping-free modeling of the Carina dSph has yet been attempted (several studies have tried to match other dSphs with more limited data sets, but Carina is currently the system with the most extended radial coverage, besides the Sgr dSph), so it remains to be seen whether such models can successfully match these observations as closely and with as much simple elegance as tidal disruption models.¹³

¹³ Wu (2007) has created multicomponent dSph models that produce both

4.6. *Misperception 6: Dark Matter and Tidal Disruption in dSphs are Mutually Exclusive*

Previous investigations of tidal effects in dSphs have often proceeded with an “all or nothing” approach with regards to the dark matter content of these systems. For example, Kuhn (1993), Fleck & Kuhn (2003), PP95, OLA95, Kroupa (1997) and Gómez-Flechoso & Martínez-Delgado (2003), all explored dark-matter-less systems, while most of the references in the previous subsection generally sought to explain the outer properties of dSphs (most often the dynamical, but not necessarily the density, properties) entirely with extended dark matter halos. Our approach has been to explore dark-matter-dominated systems, but ones where tidal disruption is still a prominent feature shaping their dynamical and structural character.

Regarding the mass content and M/L of our test case, the Carina dSph, our modeling yields revealing insights:

- Carinas with no dark matter (current $M/L \sim 1 - 3$, or $M \sim 1 \times 10^6 M_{\odot}$) are hard to make: Low mass models on benign (rather circular) orbits with scale lengths comparable to real dSphs and that manage to survive (for 10 Gyr or five orbits) do not show the proper density nor velocity dispersion profile. On the other hand, low mass models on highly radial orbits are generally destroyed relatively easily (as has previously been found by PP95) and in order to make such satellites survive until the present time the initial densities have to be so high that the scale lengths are unrealistically small compared to dSphs. Moreover, during those evolutionary phases when the models still retain a bound core, the central velocity dispersion is also too low to provide an acceptable match to the data even if one resorts to the effects of binary stars or atmospheric jitter in the giant star atmospheres to account for the differences between the model and observed central velocity dispersion (see §1.1).
- On the other hand, MFL Carinas with current masses significantly higher than $3 - 4 \times 10^7 M_{\odot}$ are impossible to make conform to the observed velocity dispersion and density profiles simultaneously. They are harder to disrupt compared to lower mass satellites for a given orbit and length scale, and even when they do disrupt, the debris is often too energetic compared to the observations (§2.2). In these cases, if one tries to reproduce the Carina number density profile (by varying the mass loss rate) the models need to be put in very eccentric orbits, which, in turn, “overheat” the particles and produces velocity dispersion profiles that significantly depart from that actually seen in Carina. Equivalently, if one tries to match the velocity dispersion profile by increasing the density (and therefore produce a modest mass loss rate), then the physical scale of the satellites becomes unrealistically small.
- Our best matching models (those with initial masses of $3.6 - 3.8 \times 10^7 M_{\odot}$) independently predict present masses for Carina consistent with those derived for the real dSph from the core-fitting method ($\sim 2 \times 10^7 M_{\odot}$, Mateo et al. 1993; Muñoz et al. 2006a). At first

flat velocity dispersion profiles and breaks in the density profiles of several other dSphs with less radially extensive velocity data.

this may seem unsurprising, given that the initial mass and length scale of the model Carina were specifically tuned so that the final stage of the simulated satellite matched its observed central velocity dispersion and core radius. It might be argued that the agreement between the estimated mass of Carina (based on its central velocity dispersion) and that of the simulated model is just a reflection of the fact that our models meet (by design) the assumptions used by the core-fitting technique: a single-component, isotropic, MFL, spherically-symmetric distribution in equilibrium follows the distribution assumed by Illingworth (1976) for estimating the total mass.

But this agreement between model and observations is not trivial. While providing by design a good match to the observed *central* velocity dispersion and scale length, the masses for the best-fitting model Carinas also provide an excellent match to the velocity and velocity dispersion profiles at large radii (when represented either as a function of radial distance or position along the major axis) out to the limits of the current observations. In addition, the amount of debris released, which is also a function of the instantaneous mass content, provides a very good match to the observed number density distribution. Interestingly, the core fitting technique, applied to the model Carina, yields the proper instantaneous bound mass value even after the satellite has lost most of its initial mass, and this technique for gauging the mass only breaks down at the point of near total destruction of the satellite. At all intermediate time steps (as Tables 3 and 4 show) the central velocity dispersion effectively tracks the bound mass content of the satellite.

In the end, the ability of our best fitting model to simultaneously match all the observed properties of Carina (except, of course, the observed ellipticity, §3.2.4) leads us to the same finding as OLA95 in that the central velocity dispersion of modeled dSphs generally reflects their equilibrium value even if the satellite is undergoing significant tidal disruption; therefore core-fitting is validated as a useful mass indicator if, even in the presence of tidal disruption, dSphs are adequately represented by MFL models. In the case of Carina, we show that the dSph is well described by tidally disrupting MFL models, even though it is still a very dark matter-dominated satellite. Clearly, it is possible for dark matter-dominated models to exhibit luminous tidal disruption.

4.7. Misperception 7: The King Limiting Radius is Meaningless as a Tidal Radius Indicator

As discussed in §4.7, at present, the underlying dark matter distribution in dSphs is still unknown, and we are left only with the distribution of the luminous matter to understand the structural properties of these systems. A relevant question for the MFL models explored in this paper then is, if in fact present dSphs can be modeled well as single-component objects, does r_{lim} provide any useful information regarding the true tidal radius of the satellite?

The tidal radius of a satellite can be defined as the place at which stars within the satellite become unbound to the system and, in turn, become bound to the host galaxy. Early studies of globular clusters (von Hoerner 1957; King 1962; Oh et al. 1992) derived simple relations to estimate this boundary that

depended only on the mass of both the satellite and the host galaxy as well as the shape of the satellite orbit, but soon afterward it was appreciated that the tidal radius of a system was also a function of the type of orbit the stars within the satellite have; stars on prograde orbits are more easily stripped than stars on radial orbits, and the latter are more easily stripped than stars in retrograde orbits (Toomre & Toomre 1972; Keenan & Innanen 1975 and more recently Read et al. 2006a). Thus, it became clear that the true tidal radii of dSphs are not a well defined edge, but rather a shell-like zone. Previous N -body simulation studies (e.g., Johnston 1998; Klimentowski et al. 2007) and the simulations presented here, show that unbound debris can linger deep inside the space defined by the bound population and, at the same time, stars still bound to the satellite can remain well into the region dominated by tidal tails, effectively “blurring” the “tidal boundary” from a Roche-like surface to a population overlap zone.

Despite the impossibility to define a clear, well delineated tidal boundary, if one knows the bound mass for a satellite in a given orbit with eccentricity e , the tidal radius at perigalacticon can be estimated using (Oh et al. 1992),

$$R_{tidal} = a \left(\frac{M_{dSph}}{M_G} \right)^{1/3} \left\{ \frac{(1-e)^2}{[(1+e)^2/2e] \ln[(1+e)/(1-e)] + 1} \right\}^{1/3} \quad (4)$$

where a is the orbital semimajor axis for the satellite, and M_{dSph} and M_G are the mass of the dSph and the MW (inside a), respectively. The question is how does this compare to the King limiting radius?

Burkert (1997) tried to estimate the enclosed mass, M_{dSph} , of several dSphs (including Carina) using this equation and adopting r_{lim} as R_{tidal} . He then compared the derived M_{dSph} to the dynamical masses (those derived from core-fitting), and argued (1) that the latter masses are much too high compared to the former masses, or (2) reversing the problem, if the masses of dSphs are indeed similar to their dynamical masses, then $R_{tidal} \gg r_{lim}$ and therefore r_{lim} has no meaning as a tidal boundary. In the latter scenario, no extratidal stars should be observed in dSphs because the luminous component is effectively shielded inside a much larger tidal boundary.¹⁴

OLA95 and PP95 also explored the relation between r_{lim} and R_{tidal} and found that a satellite is able to survive tidal interaction (i.e., not be completely destroyed by tides) for several Gyrs only if its r_{lim} is smaller than twice its R_{tidal} .

The results from our survey provide us with a possible way to weigh in on the question of R_{tidal} versus r_{lim} . In Tables 3 and 4, we show the instantaneous tidal radii of our satellites as determined by equation (4) using the bound mass of the system at that point of evolution and the density of the MW at those apogalactica. As may be seen, our models meet the OLA95 conditions for luminous tidal stripping ($r_{lim} > R_{tidal}$) and survival ($2R_{tidal} > r_{lim}$) at the same time. However, our results are at odds with the conclusions of Burkert (1997): Despite having masses of a few times 10^7 (as correctly inferred by core-fitting in our models), our best fitting models have a tidal radius smaller than its r_{lim} and do show extended, *unbound* populations. This discrepant result is explained by an arithmetical mistake in the application of equation (4) by Burkert (1997).¹⁵

¹⁴ This does not preclude dSphs from having extended luminous components if these form part of an extended, bound halo.

¹⁵ While rewriting equation (4) to solve for M_G , which involves cubing the

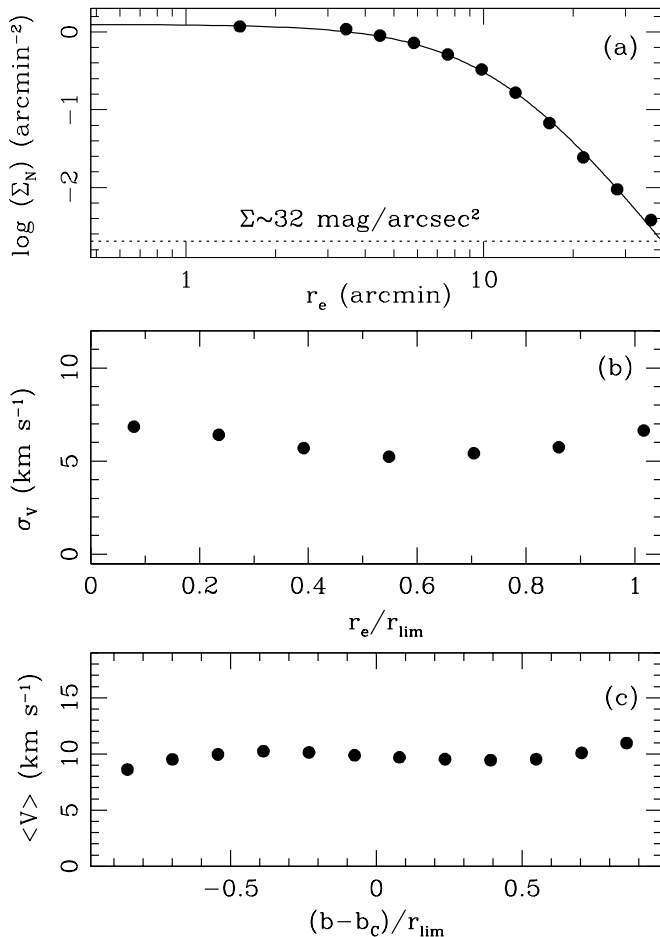


FIG. 15.— (a) Number density profile, (b) velocity dispersion versus angular distance and (c) mean RV trend along the major axis for model 502I when only particles within r_{lim} are considered. This mimics the typical surface brightness limits of “traditional” dSph photometric + spectroscopic studies. The dotted line in panel (a) represents a typical background level from photometric surveys (Majewski et al. 2005).

If single-component models undergoing tidal stripping are adequate enough that they provide a functional description to the observed properties of dSphs, then they revalidate the value of r_{lim} as at least a *crude* approximation for an upper limit for the R_{tidal} of dSph systems (i.e. $2R_{tidal} > r_{lim} > R_{tidal}$). In this regard, Majewski et al. (2003) have already argued that in the case of Sagittarius, the only dSph clearly in the process of being tidally disrupted, the true tidal radius has to be well inside r_{lim} of the light distribution.

4.8. Misperception 8: The Combined Observations of dSphs Show That They Are Not Being Tidally Disrupted

The main purpose of this work has been to demonstrate that Galactic tidal effects can produce the observed properties of dSphs, in particular, those of Carina, the Galactic dSph with the most extensive structural and kinematical data sampling to date, but otherwise a system not unusual compared to most

equation, Burkert (1997) did not cube the expression within the braces on the right-hand side where the effect of the orbital eccentricity e is included. The error becomes increasingly significant as the orbital eccentricity of a system increases, but even the value of the expression for the case where $e = 0$ is incorrectly reported in that paper.

other dSphs in its structure and dynamics. We have also previously reported that the Leo I dSph is well-fitted by tidal disruption models (Sohn et al. 2007), and possesses characteristics (an asymmetric velocity distribution at large radius) that cannot be readily explained by an extended dark halo. Recently, Mateo, Olszewski, & Walker (2007) reported a rotational signal in the outer parts of Leo I they interpret as the signature of tidal stripping, in line with our arguments for Leo I. While the Sgr dSph is an uncontroversial case of a dSph in the process of being accreted, there is a tendency to attribute Sgr (Mateo 1998, Gilmore 2004), and now Carina as well (Gilmore et al. 2007), as “exceptions to the rule” that dSphs are in general not disrupting. The results presented here suggest that it is not straightforward to argue against this position with current data on dSphs other than Sgr because, even if dSphs are undergoing significant tidal stripping, the effects can be for the most part undetectable (e.g., §4.3).

To illustrate how the lack of sufficiently sensitive data can devolve into an apparently definitive argument against tidal disruption we use recent discussions regarding the state of the Draco dSph galaxy. The lack of concordance between observational results and expectations from previous N -body simulations have been used to conclude that Draco cannot be significantly tidally influenced by the MW. The main arguments supporting this view are summarized by Kley et al. (2001), who argue that Draco cannot be significantly affected by Galactic tides because: (1) no significant rotation is observed within the radial extent of the current kinematical surveys (which are limited to Draco’s r_{lim}), (2) Draco shows a “roundish” appearance (low eccentricity of ~ 0.3) in apparent contradiction with the predictions of the N -body simulations done by PP95 and OLA95, and (3) its surface brightness profile is adequately fitted by a Plummer law without the need to resort to an “extended” population in the outer parts.¹⁶ Furthermore, Odenkirchen et al. (2001) add that no tidal tails from Draco are visible within the SDSS data and Read et al. (2006b) argue that tidal stripping of dSphs should cause the velocity dispersion profile to rise rather than to remain flat, which is the observed behavior for Draco.

While not claiming by any means that Draco is being tidally disrupted, we have shown in this paper that an object with Draco’s observed structure and kinematics can still be experiencing tidal stripping of its luminous matter. To illustrate further how this fact may be disguised, Figure 15 shows the density profile, velocity dispersion profile and RV trend (in GSR) of one of our best matching model Carinas, but with data “observed” only out to r_{lim} , as is the case for Draco (compare to Figure 10, where the full model data are shown).¹⁷ Carina and Draco are at nearly similar distances (80 vs 100 kpc), have similar sizes, similar luminosities and both have high central M/L . However the two dSphs have different v_{GSR} , with the velocity suggesting a vastly larger apogalacticon for Draco; nevertheless our Carina model is useful for this illustrative exercise.

In Figure 15a we show that, as observed in the case of Draco, a Plummer model does an excellent job fitting the photometry, even though, in fact, the outer parts of the model density profile are dominated by debris and the bound component

¹⁶ More recently, Wilkinson et al. (2004) found that the surface brightness profile of Draco seems to show a “break” at about $25'$, which is inside its observed r_{lim} , whereas Segall et al. (2007) could not confirm the presence of this extended population down to three orders of magnitude below the central number density.

¹⁷ The kinematical data on Draco in fact barely reaches its r_{lim} .

has departed from the initial Plummer distribution. Figure 15b shows that the velocity dispersion profile does not significantly increase beyond the central value within the radial extent of our “observations”, a result that contradicts the above Read et al. (2006b) claim for the expected rising behavior of the dispersion profile used to argue against tidal disruption in Draco. Figure 15c shows that no statistically significant rotation is observed within the nominally probed Draco radius, where significant means greater than the velocity dispersion (Pryor 1996). Finally, the intrinsic eccentricity of the bound component of the model, as “observed” in Figure 11, is close to zero. Both of these latter findings are also contrary to arguments by Kley et al. (2001) against Draco disruption, arguments based on expectations from the models developed by OLA95 and PP95.

Taken together, the Figure 15 “observations” of a tidally disrupting (fractional mass loss rate of 0.1 per Gyr), MFL satellite model — when coupled with common misperceptions regarding the expected characteristics of such structures — can be used to argue compellingly that our model satellites are neither tidally disrupting nor well-explained by MFL models. With this apparent “failure of the tidal model” (Klessen, Grebel, & Harbeck 2003), it is understandable how searches for an alternative mechanism to explain the flat Draco velocity dispersion profile would be deemed unnecessary or irrelevant.

5. FINAL REMARKS

5.1. *What Other Studies Are Saying*

As mentioned in the Introduction, the OLA95 and PP95 studies provided important benchmarks in the exploration of the structure and dynamics of dSph galaxies, but in many ways the results of these studies have been taken out of context and extrapolated to regimes that, we believe, were not actually intended by these authors. *The primary emphasis of these two studies was to establish whether tides could inflate the central velocity dispersions of dSph galaxies as a way to eliminate the necessity of dark matter; the goal of these studies was not to rule out that any tidal effects could be occurring in dSph satellites.* Even though PP95 and OLA95 succeeded in demonstrating that in fact tidal effects *don't* typically inflate central velocity dispersions (a result we have also found here), it doesn't follow that tidal disruption is not happening in dSph systems. Nor is it appropriate to take the observed effects in the very well-defined and restricted range of the PP95 and OLA95 simulations and apply them generally to other contexts.

For example, perhaps the most cited broadside used to sink the tidal disruption proposition is the lack of observed dSph rotation, — e.g., from Koch et al. (2007b) : “... the most efficient way of gathering evidence whether a particular dSph is being affected by tides sufficiently strongly that its kinematics are being modified is to look for any sign of apparent rotation in its outer regions.” This leads to arguments against tides not only in particular dSphs — e.g., “all in all, there is no kinematical evidence of any significant velocity gradients in Leo II, either due to rotational support or produced by Galactic tides. It therefore appears that tides most likely have not affected Leo II to any significant degree...” (Koch et al. 2007b) — but against tides generally in Local Group dwarf galaxies, since “...to date, all but one of the dSphs of the Local Group show no significant velocity gradients.” But our analysis of this manifestation of tidal disruption (§3.1.2 and §4.1) shows

clearly that rotation is not a reliable test of tidal disruption — a result that, in hindsight, should not be that surprising since (1) PP95 *already had demonstrated that the effect was pronounced in only a limited set of circumstances* (e.g., at perigalacticon, or when the MW is modeled as a point mass), (2) both PP95 and OLA95 stress that this phenomenon would be visible only at very large radii (i.e., outside the tidal radius, typically on > 1 deg scales) where few dSphs have been explored, and (3) with small amplitude in most cases.

Meanwhile, in addition to the rotation argument, Gilmore et al. (2007) suggests that *flat dispersion profiles also argue against tidal disruption*: “...there is some evidence ... for flat velocity dispersion profiles to large distances (Sohn et al. 2007; Muñoz et al. 2005), ... which are inconsistent with simple tidal disruption effects, particularly since most dSphs show no evidence of apparent rotation (Koch et al. 2007a).” But of course, in addition to our modeling here, tidal disruption models have already been demonstrated to be capable of producing flat dispersion profiles in a number of studies in preceding years (PP95; Kroupa 1997; Mayer et al. 2002) — including in the very Sohn et al. study referenced in the above passage. Indeed, the dominating influence of unbound stars on the velocity dispersion at large radius is one of the very reasons MFL tidal disruption models have been invoked (at least by our group — e.g., Law et al. 2005; Sohn et al. 2007) as a potential dSph scenario. In actuality, it is *only* in this circumstance that such models *could* work, for, as summarized by Gilmore et al. (2007): “More generally, there are unavoidable consistency requirements in any mass follows light model. In any model where mass follows light the projected velocity dispersion must be maximum at the centre, and then fall monotonically. For a well-mixed (star cluster) system, the velocity dispersion will decrease by roughly a factor of two over three core radii. This is an unavoidable requirement for any mass follows light system, and is observed in star clusters ... Such a velocity dispersion profile is not required by data in any well studied galaxy, however small, further emphasising the intrinsic difference between (virial, King) star clusters and galaxies.” The latter description as written is obviously correct *in the absence of tidal effects*, but it should not be used as an argument against MFL models when they are being used to explore the very regime — tidal disruption — to which the statement is *not* applicable.

Perhaps another unfortunate aftermath to the PP95 and OLA95 papers is that, by their example of exploring *completely dark-matter-free* satellites, these two studies may have had an unintended and undue influence in paralyzing subsequent discussions into considering primarily two polarized viewpoints or modeling strategies — namely, those where (1) the model satellites have *no* dark matter (thus requiring some reassessment or proposed revision of the physics involved with conventional mass determinations to reconcile the DM-less hypotheses with the observations), or where (2) dark matter is invoked to be responsible for *all* observed effects seen in dSph galaxies (most starkly demonstrated by the frequent incorporation of large dark matter halos to explain the structure and dynamics of dSphs at large radii). In our opinion, and as demonstrated by the results presented in this paper, there is an enormous middle ground between these polar positions.

Nevertheless, more recently the weight of discussions has strongly tacked to the side of the large dark matter halo hypothesis to explain the structure of dSphs — to the point that there are often strongly expressed sentiments that there

simply is no longer any reason for consideration of alternative models. Ironically, this viewpoint is partly driven by, on the one hand, the apparent success of Λ -CDM in explaining structure on large scales, but on the other hand the *lack of success* of Λ -CDM in explaining structure on galaxy scales so that more massive satellites are needed to help resolve the missing satellites problem. Extended, non-MFL dark matter halos can not only account for some of the observed properties of dSph galaxies at large radii and fit into Λ -CDM paradigm, but they mitigate to some degree the mismatch in the observed and Λ -CDM-predicted mass spectrum of satellite systems. Thus, for example Wu (2007) concludes “Because our [multi-component, extended dark matter] models can fit both radial velocity profiles and surface number density profiles, the so-called ‘extra-tidal extensions’ in the surface number density profiles found by Irwin & Hatzidimitriou (1995) and Wilkinson et al. (2004) do not require any special ad hoc explanation. *Thus it is not valid to consider them as the evidence of tidal stripping*, as proposed by some authors (e.g., Martínez-Delgado et al. 2001; Gómez-Flechoso & Martínez-Delgado 2003; Muñoz et al. 2005).”¹⁸

But we have shown here that our tidally disrupting MFL models can fit *not only* the radial velocity profile and surface number density profile of the Carina dSph *but also* the velocity dispersion profile. In addition, tidal disruption is a naturally occurring, established phenomenon in the evolution of galaxies (see §5.2). Thus, the MFL models are less ad hoc than implied above and, indeed, they provide a fully self-consistent explanation for all of the structure and dynamics of at least the Carina dSph. Unfortunately, what such models are *not* consistent with is the prevailing understanding of dark matter, wherein the latter is non-baryonic and does not strongly couple with luminous matter. Thus it is not clear *why* mass should follow light.

On the other hand, while multi-component models are aligned with the Λ -CDM orthodoxy, there are, as yet, no specific predictions in the context of dSphs from Λ -CDM theory for the expected structure and dynamics of the luminous matter embedded in dark halos. Indeed, the inability to predict both the observed cored profiles and the angular momentum distributions of galaxies are acknowledged additional failings of CDM on galactic scales (e.g., Navarro & Steinmetz 2000a,b), and multi-component models of dSphs *must also* adopt empirically-based, ad hoc distributions for the luminous matter, such as King profiles (e.g., Strigari et al. 2007; Peñarrubia, Navarro, & McConnachie 2007).

Clearly then each the MFL and multi-component models have unsatisfying philosophical aspects and neither can account for *why* luminous matter should organize in a particular way in the presence of substantial dark matter; under such circumstances we believe it is pertinent to address more basic questions such as “Which model works better?” or “Can a given model be definitively ruled out?”. One of the goals of this paper is to try to “clear the air” with regard to (MFL) tidal disruption models, i.e. to clarify their expected characteristics over a wider (and more likely) range of parameter space than previously explored, so that, ultimately, stronger tests can be developed for either verifying the tidal disruption hypothesis or ruling it out. Ironically, while we can make testable predictions for the tidal disruption hypothesis that can be checked with the discovery and observations of dSph stars at ever large

radii, there is no direct way to check extended dark matter models at large dSph radii, beyond where there are sufficient luminous tracers and where most of the dark matter halo is supposed to lie. In this sense the extended dark matter models are virtually unconstrained, because the extent and mass of the dark matter halos depends strongly on how one constructs the mass function (or v_{circ} distribution function) beyond the light. And, even at radii where some stars are present, with extra free parameters at their disposal, multi-component models can usually be constructed to accommodate the properties of those stars. Perhaps this is why tidal disruption models are “more vulnerable” in the common discourse on dwarf galaxies: Whereas the challenging exercise of discovering dSph-associated stars at large radii is the *sine qua non* of the tidal disruption scenario, extended dark matter halo theories are essentially immune to whether stars are found at large radius or not. At this point it seems that virtually the only way to *disprove* the existence of an enormously extended dark matter halo around any particular dSph is to push the discovery of associated stars to *reductio ad absurdum* radial limits where unreasonable dSph masses are needed to keep the stars bound to the satellite (a strategy employed in, e.g., Muñoz et al. 2005, 2006a).

5.2. What We Are Saying and What We Are Not Saying

In this paper we attempted to go beyond the seminal PP95 and OLA95 papers to explore tidal disruption models across a wider, and we believe more realistic, part of the parameter space of satellite mass, density, and orbit. Like these landmark papers, we used one component models, but with a key difference in that we adopt satellite masses consistent with dSphs having significant dark matter contents — i.e. consistent with the central mass-to-light ratios.

Remarkably, despite the simplicity of our models, which by virtue of having a single dynamical component invoke the minimum number of free parameters (satellite mass, linear scale, and orbit), we have been able to zero in on examples that rather faithfully reproduce Carina’s velocity profile, velocity dispersion profile, density distribution and other properties over its entire sampled radius, and without appealing to special timing or other particular viewing conditions (except that the satellites match the current properties of the real Carina system). We have previously also successfully modeled the properties of the Leo I dSph system using similar techniques (Sohn et al. 2007).¹⁹ In both cases, the defining characteristic of the successful family of models is high orbital eccentricity. And in both cases the central velocity dispersion is found to faithfully represent the bound mass and central M/L of the parent satellite (40 and 5, respectively, for Carina and Leo I), while the properties of the outer part of the satellite (the density law, velocity profile, and velocity dispersion profile) are strongly influenced by the presence of unbound tidal debris. But, far from being *ad hoc*, as characterized and dismissed by Wu (2007), this tidal debris is a *natural consequence* of the dynamical evolution of the satellite and, moreover, *it represents a phenomenon already observed in Nature*: Indeed, were one to subscribe to the Principle of Parsimony, a successful one component model would be *preferred* over an equally successful multi-component model,

¹⁹ We have used these techniques to model the Sgr dSph system (Law et al. 2005) as well, but in this case the focus was less on matching the properties of the parent satellite core and more on adequately explaining the properties of the tidal debris.

¹⁸ Emphasis added.

which could be argued to contain superfluous elements²⁰.

Our own position regarding the implications of the simulations presented in this paper takes into account not only the practical success of tidally disrupting, MFL models in describing at least some specific MW dSph systems, but several additional, more general observations:

1. Both dark matter and tides exist in the Universe. Tidal effects are expected in CDM models (e.g., Hayashi et al. 2003; Kazantzidis et al. 2004; Kravtsov, Gnedin & Klypin 2004; Bullock & Johnston 2005; Knebe et al. 2006).
2. The degree of importance of tides must surely vary among Galactic satellites, being a function of the structure of the satellites and the nature of their orbits.
3. We see tidal debris streams throughout the Galactic halo, some of them massive or dynamically warm enough to have come from the disruption of dwarf galaxies (Newberg et al. 2002; Majewski et al. 2004; Duffau et al. 2006; Grillmair & Dionatos 2006b; Grillmair 2006; Belokurov et al. 2007).
4. There are growing suggestions of apparent tidal effects among MW dSphs besides Sagittarius, Carina and Leo I, including most recently in the Ursa Major (Willman et al. 2005, 2006), Ursa Major II (Zucker et al. 2006b; Fellhauer et al. 2007), Canes Venatici (Zucker et al. 2006a), Boötes (Belokurov et al. 2006), and Hercules (Coleman et al. 2007) systems.

A theory for the structure and evolution of dSph galaxies that can also account for the above, generally non-controversial elements in a natural way would have the appeal of an overall economy of hypothesis.

While we have not ruled out large dark matter models and our N -body simulations are by no means intended to be unique descriptions of the Carina dSph in particular, or dSphs in general, we hypothesize that at least *some* present dSphs might actually be well represented by tidally disrupting, MFL models. This hypothesis is not incompatible with Λ -CDM, and it is not our intention to argue against Λ -CDM or extended dark matter halos in general. It would be foolish to do so, for it is virtually impossible to prove that extended dark halos do not exist, whereas, as we have discussed in §4, it is *very* difficult to prove that tidal disruption *is* happening in most dSphs. Under these circumstances, the most conservative position is to say that both possibilities might coexist.

For example, if most luminous galaxies start out embedded in extended dark subhalos of various relative sizes, eventually those on more disruptive orbits and/or with lower densities and/or radial extents will have their dark matter cloaks whittled down by tidal mass loss until their luminous matter is “exposed” and vulnerable to the same tidal effects (creating visible tidal debris streams). Indeed, Klimentowski et al. (2007) show that cosmologically-driven galaxy formation

models with two-component satellites that also experience tidal disruption naturally lead to the evolution of MFL-like satellites after their extended dark matter halos have been stripped down to the luminous cores, and at the present time a certain fraction of Galactic subhalos can be expected to be in this state. Thus, *the Carina dSph didn't necessarily start out as an MFL-like satellite*, even if it might be as one now. Other dSphs, such as Draco, might still be firmly enshrouded within extended dark matter cocoons (Łokas 2002; Kleyna et al. 2002; Mashchenko et al. 2005; Segall et al. 2007; Wu 2007), although, again, as pointed out in §4.9 and Figure 15, were Draco in a tidally disrupting phase it could be extremely difficult to prove. dSphs like Ursa Minor (Martínez-Delgado et al. 2001; Palma et al. 2003; Muñoz et al. 2005) and Leo I (Sohn et al. 2007) might be in states similar to Carina as we have modeled it here, whereas other systems, such as Sgr and perhaps some of the newly found, extremely low luminosity dSphs with evidence of tidal disruption (e.g., Ursa Major I and II, Canes Venatici, Boötes, Hercules) may be farther along this path of metamorphosis. Fellhauer et al. (2007) have already shown explicitly that Ursa Major II — the apparent progenitor of the “Orphan” stream (Belokurov et al. 2007) — is better described by a single-component than a two-component structural model, in keeping with the general scenario outlined here. Finally, we might expect there to be some systems now completely destroyed, and visible only by their tidal debris. Such debris might be in well-correlated tidal streams, or more diffuse “clouds”, depending on the details of the satellite-MW interaction. Indeed, we have produced some N -body models for systems that are of low mass, low density satellite on highly radial orbits that are completely destroyed, and the remains of these systems resemble the large, diffuse, halo “star cloud” recently discovered in Triangulum-Andromeda by Rocha-Pinto et al. (2004) and Majewski et al. (2004). Other features, like the “shelves” of stars seen around the disk of M31, can be created as tidal shells by very intense satellite-host interactions (Fardal et al. 2006; Gilbert et al. 2007).

Whether such a unified dSph evolutionary scenario might conflict with standard CDM models can be tested by comparing the predicted versus actual number of systems in each of the above evolutionary states. As shown by S. R. Majewski et al. (in preparation), tidal disruption and Λ -CDM are only *forced* into confrontation should it be found that *too many* MW dSphs can be well represented by MFL, tidally disrupting systems.

We thank an anonymous referee for her/his useful comments that helped improve this paper. RRM and SRM acknowledge funding by NSF grant AST-0307851, NASA/JPL contract 1228235 for the SIM PlanetQuest Key Project *Taking Measure of the Milky Way*, the David and Lucile Packard Foundation, and the generous support of Frank Levinson through the Celerity Foundation. KVJ acknowledges support from an NSF CAREER Award, AST-0133617 as well as support from the same NASA/JPL contract above.

Contra Gentiles, from the *Basic Writings of St. Thomas Aquinas*, translated by A.C. Pegis, Random House, New York, 1945, p. 129).

REFERENCES

- Armandroff, T. E., Olszewski, E. W., & Pryor, C. 1995, *AJ*, 110, 2131
- Aaronson, M. 1983, *ApJ*, 94, 657

- Bellazzini, M., Fusi Pecci, F., & Ferraro, F. R. 1996, MNRAS, 278, 947
- Belokurov, V., et al. 2006, ApJ, 647, L111
- Belokurov, V., et al. 2007, ApJ, 658, 337
- Bizyaev, D., et al. 2006 AJ, 131, 1784
- Bullock, J. S., & Johnston, K. V. 2005, ApJ, 635, 931
- Burkert, A. 1997, ApJ, 474, L99
- Carney, B. W., Latham, D. W., Stefanik, R. P., Laird, J. B., & Morse, J. A. 2003, AJ, 125, 293
- Coleman, M. G. et al. 2007, ApJ, *submitted* (arXiv:0706.1669)
- Coleman, M. G., Da Costa, G. S., & Bland-Hawthorn, J. 2005, AJ, 130, 1065
- Combes, F., Leon, S., & Meylan, G. 1999 A&A, 352, 149
- Choi, P. I., Guhathakurta, P., & Johnston, K. V. 2002, AJ, 124, 310
- Cuddeford, P., & Miller, J. C. 1990, MNRAS, 224, 64
- Duffau, S., Zinn, R., Vivas, A. K., Carraro, G., Méndez, R. A., Winnick, R., & Gallart, C. 2006, ApJ, 636, L97
- Eskridge, P. B. 1988a, AJ, 95, 1706
- Eskridge, P. B. 1988b, AJ, 96, 1352
- Fardal, M. A., Guhathakurta, P., Babul, A., & McConnachie, A. W. 2006, MNRAS, *submitted* (astro-ph/0609050)
- Fellhauer, M. et al. 2007, MNRAS, 375, 1171
- Fleck, J., & Kuhn, J. R. 2003, ApJ, 592, 147
- Gerhard, O. E., & Spergel, D. N. 1992, ApJ, 397, 38
- Ghigna, S., Moore, B., Governato, F., Lake, G., Quinn, T., & Stadel, J. 1998, MNRAS, 300, 146
- Gilbert, K. M., et al. 2007, ApJ, *in press* (astro-ph/0703029)
- Gilmore, G. 2004, in "Milky Way Surveys: The Structure and Evolution of our Galaxy", ASP Conference Proceedings Vol. 317, eds. D. Clemens, R. Shah, & T. Brainerd (San Francisco: ASP), 239
- Gilmore, G., Wilkinson, M. I., Kleyana, J. T., Koch, A., Evans, N. W., Wyse, R. F. G., & Grebel, E. K. 2006, (astro-ph/0608528)
- Gilmore, G., Wilkinson, M. I., Wyse, R. F. G., Kleyana, J. T., Koch, A., Evans, N. W., & Grebel, E. K. 2007, ApJ, 663, 948
- Goerdt, T., Moore, B., Read, J. I., Stadel, J., & Zemp, M. 2006, MNRAS, 368, 1073
- Gómez-Flechoso, M. A., Fux, R., & Martinet, L. 1999, A&A, 347, 77
- Gómez-Flechoso, M. A., & Martínez-Delgado, D. 2003, ApJ, 586, L123
- Grillmair, C. J., & Dionatos, O. 2006a, ApJ, 641, L37
- Grillmair, C. J., & Dionatos, O. 2006b, ApJ, 643, L17
- Grillmair, C. J. 2006, ApJ, 645, L37
- Hargreaves, J. C., Gilmore, G., Irwin, M. J., & Carter, D. 1994, MNRAS, 269, 957
- Hargreaves, J. C., Gilmore, G., & Annan, J. D. 1996, MNRAS, 279, 108
- Hayashi, E., Navarro, J. F., Taylor, J. E., Stadel, J., & Quinn, T. 2003, ApJ, 584, 541
- Hernquist, L., & Ostriker, J. P. 1992, ApJ386, 375
- Hodge, P. W. 1961a, AJ, 66, 249
- Hodge, P. W. 1961b, AJ, 66, 384
- Hodge, P. W. 1962, AJ, 67, 125
- Hodge, P. W. 1966, AJ, 71, 204
- Hodge, P. W., & R. W. Michie 1969, AJ, 74, 587
- Illingworth, G. 1976, ApJ, 204, 73
- Irwin, M., & Hatzidimitriou, D. 1995, MNRAS, 277, 1354
- Johnston, K. V., Hernquist, L., & Bolte, M. 1996, ApJ, 465, 278
- Johnston, K. V. 1998, ApJ, 495, 297
- Johnston, K. V., Sigurdsson, S., & Hernquist, L. 1999a, MNRAS, 302, 771
- Johnston, K. V., Zhao, H., Spergel, D. N., & Hernquist, L. 1999b, ApJ, 512, L109
- Kauffmann, G., White, S. D. M., & Guiderdoni, B. 1993, MNRAS, 261, 201
- Kazantzidis, S., Mayer, L., Mastrogiro, C., Diemand, J., Stadel, J., & Moore, B. 2004, ApJ, 608, 663
- Keenan, D. W., & Innanen, K. A. 1975, AJ, 80, 290
- King, I. R. 1962, AJ, 67, 471
- King, I. R. 1966, AJ, 71, 64
- Klessen, R. S., & Kroupa, P. 1998, ApJ, 498, 143
- Klessen, R. S., & Zhao, H. 2002, ApJ, 566, 838
- Klessen, R. S., Grebel, E. K., & Harbeck, D. 2003, ApJ, 589, 798
- Kleyana, J. T., Geller, M. J., Kenyon, S. J., & Kurtz, M. J. 1999, AJ, 117, 1275
- Kleyana, J. T., Wilkinson, M. I., Evans, N. W., & Gilmore, G. 2001, ApJ, 563, L115
- Kleyana, J. T., Wilkinson, M. I., Evans, N. W., Gilmore, G., & Frayn, C. 2002, MNRAS, 330, 792
- Kleyana, J. T., Wilkinson, M. I., Gilmore, G., & Evans, N. W. 2003, ApJ, 588, L21
- Kleyana, J. T., Wilkinson, M. I., Evans, N. W., & Gilmore, G. 2004, MNRAS, 354, L66
- Kleyana, J. T., Wilkinson, M. I., Evans, N. W., & Gilmore, G. 2005, ApJ, 630, L141
- Klimentowski, J., Łokas, E. L., Kazantzidis, S., Prada, F., Mayer, L., & Mamon, A. 2007, MNRAS, 378, 353
- Klypin, A., Kravtsov, A. V., Valenzuela, O., & Prada, F. 1999, ApJ, 522, 82
- Knebe, A., Power, C., Gill, S. P. D., & Gibson, B. K. 2006, MNRAS, 368, 741
- Kroupa, P. 1997, New Astronomy, 2, 139
- Koch, A., Wilkinson, M. I., Kleyana, J. T., Gilmore, G. F., Grebel, E. K., Dougal, M. A., Evans, N. W., & Wyse, R. F. G. 2007a, ApJ, 657, 241
- Koch, A., Kleyana, J. T., Wilkinson, Grebel, E. K., Gilmore, Evans, N. W., Wyse, R. F. G., & Harbeck, D. R. 2007b, AJ, 134, 566
- Kravtsov, A. V., Gnedin, O. Y., & Klypin, A. A. 2004, ApJ, 609, 482
- Kuhn, J. R., & Miller, R. H. 1989, ApJ, 341, 41
- Kuhn, J. R. 1993, ApJ, 409, L13
- Kuhn, J. R., Smith, H. A., & Hawley, S. L. 1996, ApJ, 469, L93
- Law, D. R., Johnston, K. V., & Majewski, S. R. 2005, ApJ, 619, 807
- Łokas, E. L. 2001, MNRAS, 327, L21
- Łokas, E. L., 2002, MNRAS, 333, 697
- Łokas, E. L., Mamon, G. A., & Prada, F. 2005, MNRAS, 363, 918
- Majewski, S. R., Ostheimer, J. C., Patterson, R. J., Kunkel, W. E., Johnston, K. V., & Geisler, D. 2000, AJ, 119, 760 (Paper II)
- Majewski, S. R., Skrutskie, M. F., Weinberg, M. D., & Ostheimer, J. C. 2003, ApJ, 599, 1082
- Majewski, S. R., Ostheimer, J. C., Rocha-Pinto, H. J., Patterson, R. J., Guhathakurta, P., & Reitzel, D. 2004, ApJ, 615, 738
- Majewski, S. R., et al. 2005, AJ, 130, 2677
- Martínez-Delgado, D., Alonso-García, J., Aparicio, A., & Gómez-Flechoso, M. A. 2001, ApJ, 549, L63
- Martin, N. F., Ibata, R. A., Chapman, S. C., Irwin, M., & Lewis, G. F. 2007, MNRAS, *in press* (arXiv:0705.4622)
- Mashchenko, S., Couchman, H. M. P., & Sills, A. 2005, ApJ, 624, 726
- Mashchenko, S., Sills, A., & Couchman, H. M. P. 2006, ApJ, 640, 252
- Mateo, M., Olszewski, E. W., Pryor, C., Welch, D., & Fischer, P. 1993, AJ, 105, 510M
- Mateo, M. L. 1998, ARA&A, 36, 435
- Mateo, M., Olszewski, E. W., Vogt, S. S., & Keane, M. J. 1998, AJ, 116, 2315
- Mateo, M. L., Olszewski, E. W., & Walker, M. G. 2007, ApJ, *in press*, arXiv:0708.1327
- Mayer, L., Governato, F., Colpi, M., Moore, B., Quinn, T., Wadsley, J., Stadel, J., & Lake, G. 2001a, ApJ, 547, L123
- Mayer, L., Governato, F., Colpi, M., Moore, B., Quinn, T., Wadsley, J., Stadel, J., & Lake, G. 2001b, ApJ, 559, 754
- Mayer, L., Moore, B., Quinn, T., Governato, F., & Stadel, J. 2002, MNRAS, 336, 119
- Mayer, L., Kazantzidis, S., Mastrogiro, C., & Wadsley, J. 2007, Nature, 445, 738
- McConnachie, A. W., & Irwin, M. J. 2006, MNRAS, 365, 1263
- Milgrom, M. 1995, ApJ, 455, 439
- Miyamoto, M., & Nagai, R. 1975, PASJ, 27, 533
- Moore, B., Ghigna, S., Governato, F., Lake, G., Quinn, T., Stadel, J., & Tozzi, P. 1999, ApJ, 524, L19
- Muñoz, R. R. et al. 2005 ApJ, 631, L137
- Muñoz, R. R. et al. 2006a ApJ, 649, 201
- Muñoz, R. R., Carlin, J. L., Frinchauboy, P. M., Nidever, D. L., Majewski, S. R., & Patterson, R. J. 2006b ApJ, 650, L51
- Navarro, J. F., Frenk, C. S., & White, S. D. M. 1997, ApJ, 490, 493
- Navarro, J. F. & Steinmetz, M. 2000a, ApJ, 528, 607
- Navarro, J. F. & Steinmetz, M. 2000b, ApJ, 538, 477
- Newberg, H. et al. 2002, ApJ, 569, 245
- Odenkirchen, M. et al. 2001, AJ, 122, 2538
- Odenkirchen, M. et al. 2003, AJ, 126, 2685
- Oh, K. S., Lin, D. N. C., & Aarseth, S. J. 1992, ApJ, 386, 506
- Oh, K. S., Lin, D. N. C., & Aarseth, S. J. 1995, ApJ, 442, 142 (OLA95)
- Olszewski, E. W., Pryor, C., & Armandroff, T. E. 1996, AJ, 111, 750
- Palma, C., Majewski, S. R., Siegel, M. H., Patterson, R. J., Ostheimer, J. C., & Link, R. 2003, AJ, 125, 1352
- Peñarrubia, J., Navarro, J. F., & McConnachie, A. W. 2007, ApJ, *in press*, arXiv:0708.3087
- Piatek, S., Pryor, C., Olszewski, E. W., Harris, H. C., Mateo, M., Minniti, D., & Tinney, C. G. 2003, AJ, 126, 2346
- Piatek, S., Pryor, C., Bristow, P., Olszewski, E. W., Harris, H. C., Mateo, M., Minniti, D., & Tinney, C. G. 2005, AJ, 130, 95
- Piatek, S., Pryor, C., Bristow, P., Olszewski, E. W., Harris, H. C., Mateo, M., Minniti, D., & Tinney, C. G. 2006, AJ, 131, 1445
- Plummer, H. C., 1911, MNRAS, 71, 460 AJ, 109, 1071

- Piatek, S., & Pryor, C. 1995, *AJ*, 109, 1071 (PP95)
- Pryor, C. 1996, *ASP Conf. Ser.* 92: Formation of the Galactic Halo...Inside and Out, 92, 424
- Read, J. I., Wilkinson, M. I., Evans, N. W., Gilmore, G., & Kleyana, J. T. 2006a, *MNRAS*, 366, 429
- Read, J. I., Wilkinson, M. I., Evans, N. W., Gilmore, G., & Kleyana, J. T. 2006b, *MNRAS*, 367, 387
- Richstone, D. O., & Tremaine, S. 1986, *AJ*, 92, 72
- Rocha-Pinto, H. J., Majewski, S. R., Skrutskie, M. F., Crane, J. D., & Patterson, R. J. 2004, *ApJ*, 615, 732
- Sanchez-Salcedo, F. J., & Hernandez, X. 2007, *in press* (astro-ph/0702443)
- Segall, M., Ibata, R. A., Irwin, M. J., Martin, N. F., & Chapman, S. 2007, *MNRAS*, 375, 831
- Sellwood, J. A., & Pryor, C. 1998, *Highlights Astron.*, 11, 638
- Siegel, M. H., Majewski, S. R., Sohn, S. T., Shetrone, M. D., & Patterson, R. 2007, *ApJ*, *submitted*.
- Smith, H. A., Kuhn, J. R., & Hawley, S. L. 1997, in *ASP Conf. Ser.* 127, Proper Motions and Galactic Astronomy, ed. R. M. Humphreys (San Francisco: ASP), 163
- Sohn, S. et al. 2007, *ApJ*, 663, 960
- Stoehr, F., White, S. D. M., Tormen, G., & Springel, V., 2002, *MNRAS*, 335, L84
- Strigari, L. E., Bullock, J. S., Kaplinghat, M., Diemand, J., Kuhlen, M., & Madau, P. 2007, *ApJ*, 669, 676
- Tolstoy et al. 2004, *ApJ*, 617, L119
- Toomre, A., & Toomre, J. 1972, *ApJ*, 178, 623
- von Hoerner, S. 1957, *ApJ*, 125, 451
- Walcher, C. J., Fried, J. W., Burkert, A., & Klessen, R. S. 2003, *A&A*, 406, 847
- Walker, M. G., Mateo, M., Olszewski, E. W., Bernstein, R. A., Wang, X., & Woodroffe, M. 2006a, *AJ*, 131, 2114
- Walker, M. G., Mateo, M., Olszewski, E. W., Pal, J. K., Sen, B., & Woodroffe, M. 2006b, *ApJ*, 642, L41
- Westfall, K. B., Majewski, S. R., Osheimer, J. C., Frinchaboy, P. M., Kunkel, W. E., Patterson, R. J., & Link, R. 2006, *AJ*, 131, 375
- Wilkinson, M. I., Kleyana, J. T., Evans, N. W., Gilmore, G. F., Irwin, M. J., & Grebel, E. K. 2004, *ApJ*, 611, L21
- Willman, B. et al. 2005, *ApJ*, 626, L85
- Willman, B. et al. 2006, *ApJ*, *submitted*. (astro-ph/0603486)
- Wu, X. 2007, *ApJ*, *submitted*. (astro-ph/0702233)
- Zucker, D. B., et al. 2006a, *ApJ*, 643, L103
- Zucker, D. B., et al. 2006b, *ApJ*, 650, L41

APPENDIX

SOME COMMENTS ON THE USE OF KING PROFILES

Although not particularly pertinent to the results of this paper, the topic of King profiles has often been linked to studies of the luminous structure of dSph galaxies. In the spirit of the overall review of dSph tidal disruption models we have presented, a few comments about King profiles seem appropriate.

Historically, King profiles (King 1962, 1966) have frequently been used to represent the stellar density distributions of dSphs (e.g., Hodge 1966; Eskridge 1988a,b; Irwin & Hatzidimitriou 1995). In this regard it is important to distinguish between King (1962) *profiles*, which are a simple empirical description of the distribution of light in a spheroidally-shaped system, and King (1966) *models*, which are physically-motivated and derived explicitly for the case of densely populated globular clusters placed in an external gravitational field. King (1966) showed that under these circumstances, his single-component models evolved naturally to the empirical profile he derived earlier for globular clusters, one whose structure can be described in terms of two linear physical scales: a core and a truncation radius (identified by King 1962 as the *tidal* radius). In globular clusters two-body stellar relaxation dominates the internal dynamics of the system and leads to the King profile in an external field, but two-body relaxation is much too inefficient in low density dSphs. Nevertheless, King profiles have frequently been found to provide an overall adequate *empirical parameterization* of the structural properties of (the most luminous, inner parts of) the light distribution in dSphs. In this usage, the outer physical scale is associated with the asymptotal radius at which the fitted two-parameter profile approaches zero (or would approach zero, in the absence of the “break population”; we have identified this *empirically-defined* radius as r_{lim} , the limiting radius, because its connection to a true tidal radius is undefined (and, indeed, one of the controversial questions about dSph structure — e.g., see §4.7).

In this paper we have used King *profiles* only in this way — as a handy empirical descriptor simply to define a *scale* for comparing the sizes of the bound central cores of our simulated satellites to each other and to the luminous inner part of Carina itself. In this case, a King profile is a logical expediency motivated by the fact that our initial particle configurations are Plummer models (i.e., non-tidally-truncated), and as they become shaped by the tidal field they come to resemble King profiles. *But none of the conclusions in this paper depend on the use of a King profile or any assumptions regarding its validity.* With the growing popularity of multi-component mass models for dSph systems, simple King *models* — designed for dense, tidally truncated, single-component systems — would naturally be considered inadequate, and, as a result, the King *profile* description has been increasingly resisted and criticized when applied to dSphs (e.g., Kleyana et al. 2001; Gilmore et al. 2006, 2007; Koch et al. 2007a; Wu 2007). Obviously, in these circumstances King models are physically meaningless: If Galactic dSphs are not single-component bodies, but rather more complex systems where the dark matter is distributed over much larger physical scales than the light, then the physical meaning of r_{lim} as a tidal truncation radius in the corresponding King profile is lost — and consequently, so too is the interpretation that “breaks” in the density distributions indicate the presence of tidal debris.

Koch et al.’s (2007a) discussion demonstrates various of the issues at play: “It has frequently been suggested in the literature that the detection of member stars well beyond the formal tidal limit radius of dSphs, canonically defined via a single-component King model representation of the observed surface brightness profiles, is evidence for physical tides. A large number of dSphs have been claimed to show hints of extratidal stars and thus tidal disruption (Irwin & Hatzidimitriou 1995; Martínez-Delgado et al. 2001; Palma et al. 2003; Muñoz et al. 2005, 2006a, 2006b). Evidence for this has also been reported for Leo I (S06). What such studies show, in fact, is that the presumed parametric fit to the measured surface brightness (and/or direct star counts) is inappropriate at large radii. Given that there is no astrophysical basis to the application of a King model to a galaxy, an astrophysical interpretation of the corresponding labels as physical processes is fraught with peril.”

Unfortunately, the above description oversimplifies the arguments made to argue in favor of the tidal disruption hypothesis by at least some of the papers they quote. For example, in the Muñoz et al. (2005, 2006a,b) papers cited above (and elsewhere), additional information — such as the dynamics of the stars, their two-dimensional sky distribution, the implied dark matter masses needed to keep the stars bound, and the fact that the radial density profiles resemble models of disrupting dSph galaxies — were also weighed into those analyses and provide more powerful and more important support for the notion that these systems

may be tidally disrupting. In the end, while the observed “breaks” in the density distributions of dSphs are not an unequivocal indicator of tidal stripping, they are at least consistent with the presence of tidal debris in the outer parts of these satellites as observed in numerous N -body simulations, even when multi-component models are used for the dSphs (e.g., Read et al. 2006b; Klimentowski et al. 2007; Peñarrubia, Navarro, & McConnachie 2007).

Finally, it is worth pointing out that there might be circumstances where King profiles (or other two-parameter density law) are actually *physically motivated* and therefore are an appropriate *physical* descriptor of dSphs. King (1962) himself addressed this issue by pointing out that his empirically derived density law is applicable to relaxed systems *regardless of the relaxation mechanism*. For example, *violent relaxation* might provide an alternative to two-body relaxation, perhaps as a process during the early formative stages of dSphs. Alternatively, as we have explored in this paper, dSphs might indeed be tidally truncated objects where their flat/rising velocity dispersion profiles are the result of tidal stripping, and thus with a truncation radius evolving in the luminous matter naturally. Such a situation may be entirely consistent with Λ -CDM expectations that these systems are (initially) embedded in larger dark matter halos, if the systems evolve to where they are reasonably described by single component models and King profiles only in the late stages of tidal evolution, after the dark outer layers of these subhalos have already been stripped away²¹ (see §5.2). Along these lines, Klimentowski et al. (2007) have shown that a two-component satellite with an initially more extended dark matter distribution can naturally evolve through tidal stripping into a system with a radial constant M/L .

²¹ It might be argued that, even after significant tidal stripping, the dark matter cocoons surrounding the dSphs’ stellar components should keep the initial, expected Navarro, Frenk, & White (NFW, 1997) density distribution. However, indirect observations show that the dark matter distribution in dSphs is more likely to be cored than cuspy (Kleyna et al. 2003; Goerdt et al. 2006; Gilmore et al. 2007).